IOWA STATE UNIVERSITY
Digital Repository

Retrospective Theses and Dissertations

Iowa State University Capstones, Theses and Dissertations

1966

# Positron annihilation in rare earth single crystals

Ronald Wendell Williams
*Iowa State University*

Follow this and additional works at: https://lib.dr.iastate.edu/rtd

 Part of the Condensed Matter Physics Commons

Recommended Citation
Williams, Ronald Wendell, "Positron annihilation in rare earth single crystals " (1966). *Retrospective Theses and Dissertations*. 3143.
https://lib.dr.iastate.edu/rtd/3143

This Dissertation is brought to you for free and open access by the Iowa State University Capstones, Theses and Dissertations at Iowa State University Digital Repository. It has been accepted for inclusion in Retrospective Theses and Dissertations by an authorized administrator of Iowa State University Digital Repository. For more information, please contact digirep@iastate.edu.

This dissertation has been
microfilmed exactly as received

67-5637

WILLIAMS, Ronald Wendell, 1939-
POSITRON ANNIHILATION IN RARE EARTH SINGLE CRYSTALS.

Iowa State University of Science and Technology, Ph.D., 1966
Physics, solid state

University Microfilms, Inc., Ann Arbor, Michigan

# POSITRON ANNIHILATION IN RARE EARTH SINGLE CRYSTALS

by

Ronald Wendell Williams

A Dissertation Submitted to the
Graduate Faculty in Partial Fulfillment of
The Requirements for the Degree of
DOCTOR OF PHILOSOPHY

Major Subject: Experimental Physics

Approved:

Signature was redacted for privacy.

In Charge of Major Work

Signature was redacted for privacy.

Head of Major Department

Signature was redacted for privacy.

Dean of Graduate College

Iowa State University
Of Science and Technology
Ames, Iowa

1966

TABLE OF CONTENTS

# INTRODUCTION

The positron, first discovered by Anderson (1) in 1932, can annihilate in a solid with an electron, either by producing gamma rays or by transferring the real energy of the two particle system to the lattice in the form of lattice vibrations, or phonons. Since the detection of the latter mode is extremely difficult and its probability of occurring is quite low, no experimental research has been carried out on phonon producing annihilations. Experimental work, on one (2,3), two, and three quantum (4,5,6) annihilations has been,however, carried out on a variety of materials.

The first experimental work on the angular correlation of two quantum annihilations was carried out in 1942 by Beringer and Montgomery (7). These investigators verified, within an accuracy of one degree, that the two photons, arising from the annihilation of positrons introduced into lead samples, were collinear. However, the poor resolution of their apparatus prevented them from making any measurement of the angular distribution of this radiation.

Since the total momentum of the annihilating pair is not, in general, zero at the time of annihilation, it should not be expected that the two gamma rays from an annihilated electron - positron system would be emitted in precisely opposite directions. In fact, the two gamma rays are not always emitted at $180^{o}$ to one another and it is this departure from collinearity

that yields valuable information about the electronic structure of a metal.

The revival of the study of angular correlation curves was begun with a paper written by DeBenedetti, Cowan, Konneker, and Primakoff (8) in 1949. In this paper the authors described an apparatus capable of resolving the basic structure of an angular correlation curve. In addition, they included the fundamental theory and demonstrated how the angular correlation curves were related to the wave functions of the electrons and, hence, to the electronic structure of metals.

In a metal the thermalization time for a positron, or the time required for a positron to reach an energy of kT, has been theoretically calculated to be of the order of $10^{-14}$ seconds (9). This time is calculated by considering the excitations of lattice vibrations after the positron has reached an energy so low that it can no longer cause interband electronic transitions. Later adjustments by Lee-Whiting (10) assume that the interaction between a positron and an electron can be, in the spirit of the Bohm - Pines theory, approximated by a screened, exponential, Coulomb potential. With this correction a thermalization time of $10^{-12}$ seconds has been calculated.

Because of the smallness of the thermal energy, kT, compared to a characteristic electronic energy of the system,

such as the Fermi energy, the positron can be considered as having reached its lowest energy state of zero crystal momentum, or its ground state, in a time of the order of $10^{-12}$ seconds. The positron, having finished losing energy by exciting electrons into higher energy bands, exists for a period of time before annihilation in its thermalized state. This phenomenon has been verified experimentally. It has been found that the mean lifetime of a positron in most metals, and in particular the rare earth metals, is near $1.5 \pm .7 \times 10^{-10}$ seconds (11,12). (The existence of two or more components of lifetimes in a metal is presently attributed to surface effects such as oxide layers or crystal imperfections.)

The question arises: which electrons will annihilate with the positrons? All electrons in a metal are capable of annihilating an entering positron, but the probability varies with the electronic state. As the positron, because of Coulomb repulsion, is almost completely excluded from the ion cores, it might be expected that most of the annihilation rate would be due to the conduction electrons. In fact, the early experimental work of DeBenedetti showed a sharp cutoff at the Fermi momentum in the momentum distribution of annihilation photons and demonstrated the large probability of the annihilations taking place between a ground state positron and a conduction electron. However, the core electrons can also be annihilated and it is these annihilation which

account primarily for the tail in the angular correlation curves (13).

The most extensive, early investigations of the angular correlation of the two annihilation photons from metals were by Stewart et al. (14,15,16) and DeBenedetti et al. (17,18). The general shapes of all the curves are smooth and approximately parabolic in the center region with tails occurring beyond the Fermi momentum cutoff. All of these investigations were carried out on polycrystalline metals.

The first measurements of the angular correlation curves from oriented single crystals were made by Berko et al. (19, 20) on graphite, copper, and aluminum. Later, Stewart et al. (21), measuring the angular correlation curves for oriented single crystals of beryllium, observed a pronounced directional dependence, for the (0001), (1120), and $(1\bar{1}00)$ directions. The observation of the anisotropic directional dependence in single crystals by Stewart et al. and the recent development in band structure calculations suggested the experimental project of this thesis: a systematic, experimental study of the angular correlation curves in single crystals of the trivalent, heavy rare earth metals with hexagonal close packed structure.

The rare earth metals are particularly well suited for study by means of positron annihilation. Although there has been a considerable amount of experimental and theoretical

work on the electrical, magnetic, and thermal properties of the rare earth metals (22-34), there has been no experimental observation of the shape of the Fermi surface in these metals reported to date. The metals are presently not pure enough for the standard types of experiment, such as the deHaas-van Alphen effect, cyclotron resonance, magnetoacoustic oscillations, anomalous skin effect, and high field galvanomagnetic effects, which have been employed in other cases to determine direct information about the shape of the Fermi surface. The metals used in this experiment were in their purest obtainable form and had resistivity ratios ($\rho_{300^oK}/\rho_{4.2^oK}$) of about 30. Most of the impurities were oxygen and tantalum. While these impurities do not appreciably affect the positron annihilation results, they reduce the mean free path of the conduction electrons so that the standard types of experiments, described above, can not be used. Present band structure calculations predict highly anisotropic Fermi surfaces (35) which should produce structure in the angular correlation curves. In addition, rare earth metals exhibit a magnetic ordering below certain characteristic transition temperatures. This magnetic ordering may introduce an additional periodicity in the Brillouin zone structure, and consequently change the Fermi surfact (36). Any large distortion of the Fermi surface due to a magnetic ordering might also be detectable in an angular correlation curve.

## EXPERIMENTAL TECHNIQUE

Because of health hazards and expense, it is convenient to limit the positron source used in an experiment of this type to approximately .1 curies. This limitation, together with a need for high resolution, requires that data be collected continuously for periods of up to two months. For this reason it is necessary to have highly regulated electronic counting equipment.

The apparatus used in this experiment was designed and built primarily by Dr. D. J. Zaffarano and Dr. D. R. Gustafson. Although the equipment has previously been described by Gustafson (37), a brief outline will be given here for the sake of completeness.

### The Source

A diagram of the holder for the positron emitter, $Co^{58}$, which was used in this experiment, is shown in Fig. 1. Although two other positron emitters, $Cu^{64}$ (12.8 hrs, EC 42%, $e^-$ 39%) and $Na^{22}$ (2.6 yrs, EC 11%) were available at the time of the experiment, it was decided that $Co^{58}$ (70 days, EC 85%) had the most desirable qualities.

$Cu^{64}$ as a positron source has the advantage of being relatively inexpensive but the disadvantage of being short lived. Consequently, even a relatively intense source of .2 curies will decay away before good statistics for forty to fifty points of an angular correlation curve can be obtained.

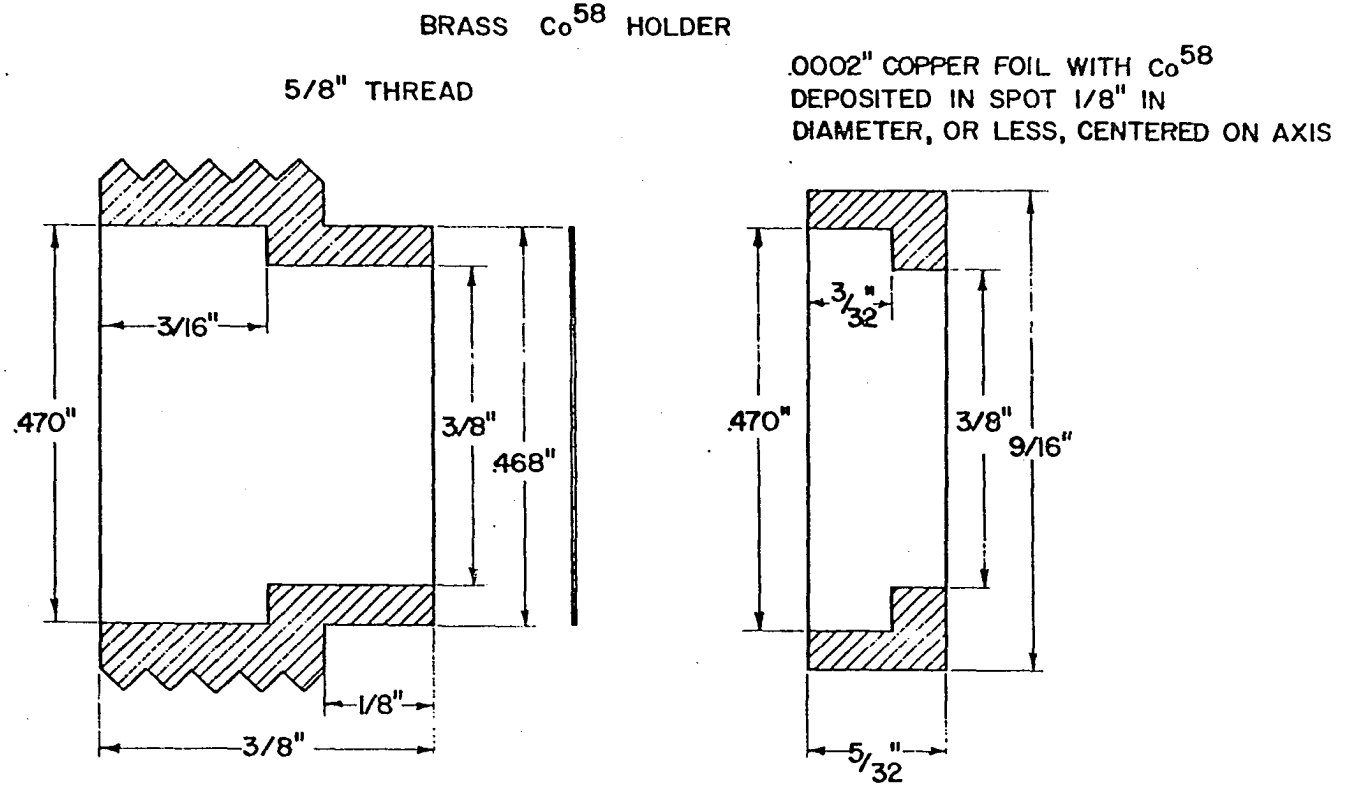


Figure 1. Diagram of the $Co^{58}$ source holder

If it is used as a positron source, its decay must be taken into account in analyzing and interpreting the data.

$Na^{22}$ has the advantage of being the source with the lowest activity per positron of the positron sources thus far mentioned. However, $Na^{22}$ is made in a cyclotron, and is, consequently, very expensive. It has the further disadvantage of coming in the form of $Na^{22}Cl$. Sources of this type must be sealed in a container to avoid accidental dispersal, and, because of annihilations in the container walls, this results in a loss of positron activity.

Like $Cu^{64}$, $Co^{58}$ has the disadvantage of a high activity per positron. However, the $Co^{58}$ has a half life long enough so that its activity does not appreciably decrease before good statistics for all points of the angular correlation curve can be obtained. Corrections due to the half life do not, therefore, have to be included in the angular correlation curves. The $Co^{58}$ is also relatively inexpensive. Three $Co^{58}$ sources were used in this experiment at an average cost of $1200 per source. Furthermore, the $Co^{58}$ can be plated on a copper foil and, because accidental dispersal of such a source is highly unlikely, it can be exposed directly to the sample without sealing.

A $Ge^{68}$ positron source, which has only recently been placed on the market, will probably be the most desirable type of source for future work of this kind. $Ge^{68}$ has a 280 day

half life and an 85% positron yield. This source can be plated on a foil and presently costs, per positron, only half as much as $Co^{58}$.

## Dewar and Slit Arrangement

In order to study positron annihilation at a variety of temperatures in a magnetic field, both the source and the sample were placed in the tail of a helium dewar. The sample, approximately 12 mm in diameter and 5 mm thick, was glued with G.E. type 7031 adhesive to a copper rod. The copper rod was thermally attached to the bottom of the helium can of the dewar. The source was placed facing the sample and the positrons were focused on the face of the sample by an external 10 kilogauss Varian magnet having a field gradient of 1 kilogauss/cm. This gradient was obtained by having one pole face of the magnet tapered to a point and the other pole face milled flat. The magnet was powered by a Varian V-2600 regulated power supply capable of regulating the current to one part in $10^5$.

The high resolution of this equipment was obtained by collimating the sample's radiation with a system of lead slits, shown in Fig. 2. Slits 2 and 3 were used so that only the radiation from the sample, and not the direct radiation of the source, could be detected, unattenuated, by the two NaI crystals placed at either end of the room. Slits 1 and 2 were stationary, and mounted with the dewar system, which

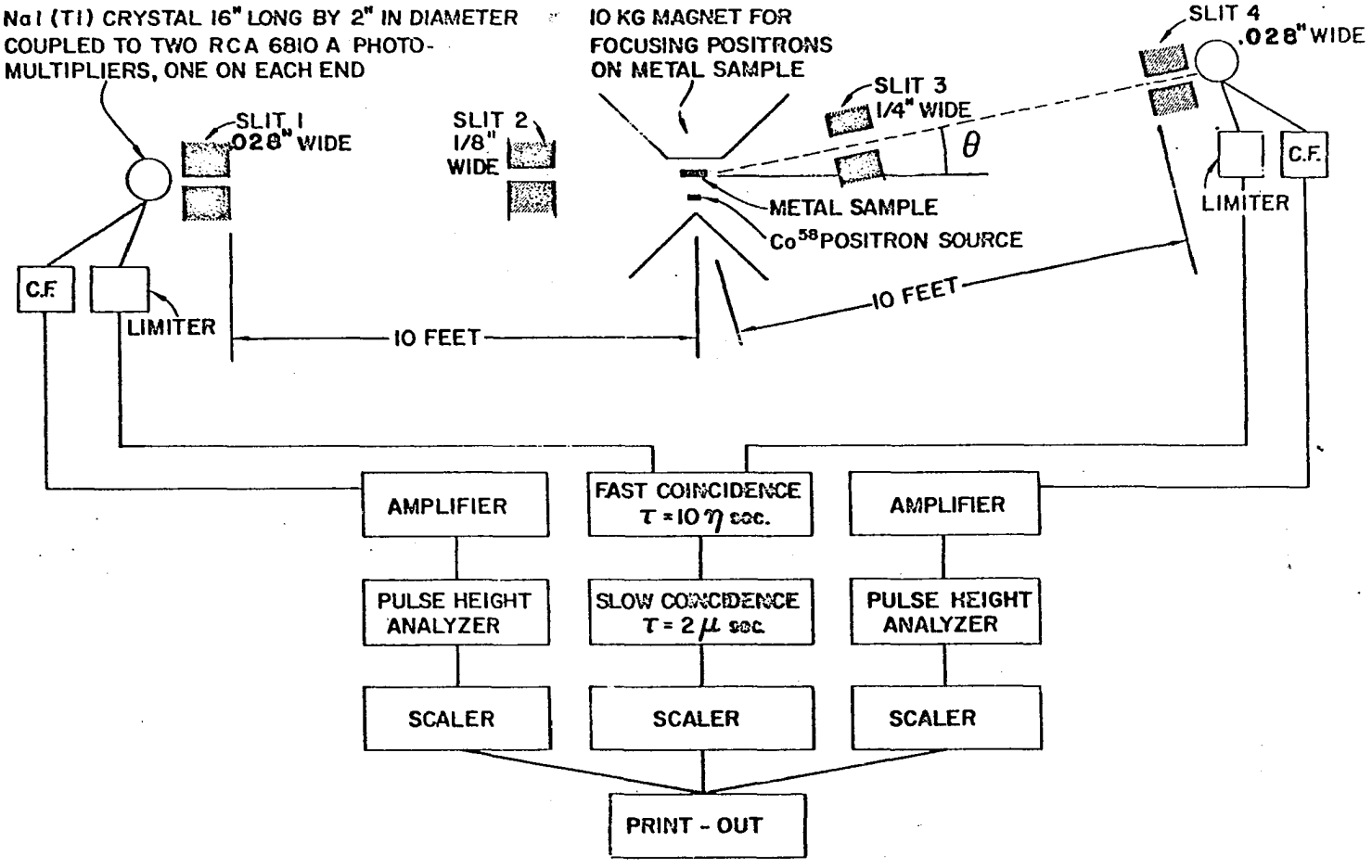


Figure 2. Block diagram of the experimental apparatus

included the source and sample. Slits 3 and 4 were mounted on a movable arm which pivoted about an axis through the sample. The detection crystals were shielded by slits 1 and 4 which were placed ten feet from the sample and with slit 4 mounted on the movable arm. Both slits 1 and 4 had their faces milled flat and separated at the top and bottom by .028 inch stainless steel shim stock. This separation defined an angle of slightly less than $\frac{1}{4}$ milliradian with respect to the sample.

The crystals used in this experiment were furnished by Harshaw Chemical Corporation and made by optically coupling two eight inch long by two inch diameter NaI(Tl) scintillation crystals. The two crystals were then encapsulated in a thin-walled aluminum cylinder fitted with optically coupled glass windows at each end of the cylinder. This functioned as an effective sixteen inch long by two inch diameter NaI(Tl) crystal and was used as a single detector. Two such detectors were used: one behind slit 1 and one behind slit 4. The light pulses occurring in the detector crystal were viewed by two 6810A RCA photomultipliers. The gains of these two photomultipliers were matched and summed.

Highly regulated Keithley model 241 power supplies were used in the experiment. A highly regulated power supply was needed to minimize drift in the pulse height from the crystals. A diagram of the resistor string for one of the four tubes is shown in Fig. 3. This diagram shows how each tube was pro-

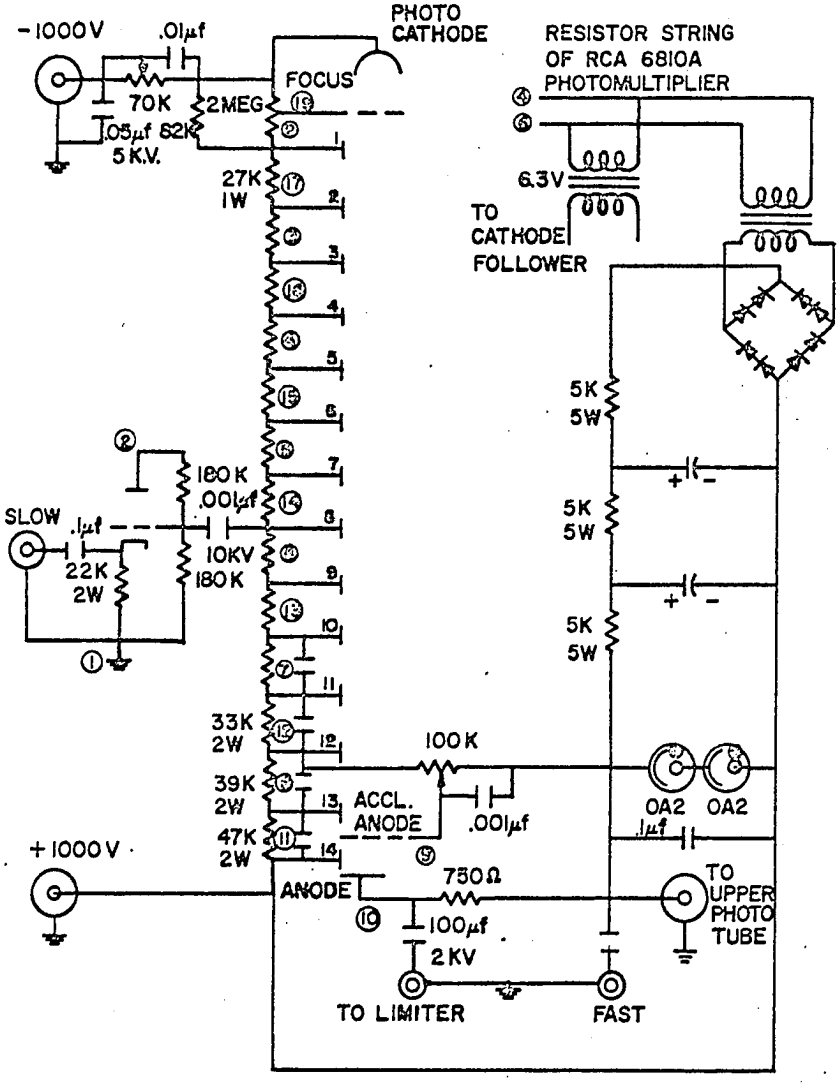


Figure 3. Diagram of the resistor string and cathode follower circuit for one of the RCA 6810A photomultiplier tubes

vided with individual gain, focus, and acceleration controls so that the performance of each tube could be optimized individually. Figures 4 and 5 show the limiter circuit and the fast coincidence circuit. The pulses from the eighth dynode of the photomultiplier tube on one end of the NaI crystal were fed into a cathode follower circuit and then summed with the pulses from the cathode follower circuit of the photomultiplier tube on the other side of the NaI crystal. The summed pulse was then fed into a Hamner N338 amplifier and pulse height analyzer. Those pulses corresponding to an energy range of approximately .3 mev to .6 mev were selected. The pulses from the anodes of the same two tubes were summed and then fed into a limiter circuit which had an output of flat top pulses of one volt with a rise time of 10 $\eta$sec. The pulses from the two limiters associated with slits 1 and 4 were then fed to a fast coincidence circuit with a 10 $\eta$sec resolving time. The output of this circuit was then fed into a Hamner N330 pulse height selector, where the level was set to discriminate fast coincidence pulses from the low level output noise of the fast coincidence circuit. The output of the two Hamner N338 amplifiers and the output of the Hamner N330 P.H.S. were then fed into a slow coincidence circuit with a resolving time of 2$\mu$ sec. The net effect was that pulses occurring in both counter crystals within 10 $\eta$sec were coincidenced with pulses of .3 mev to .6 mev

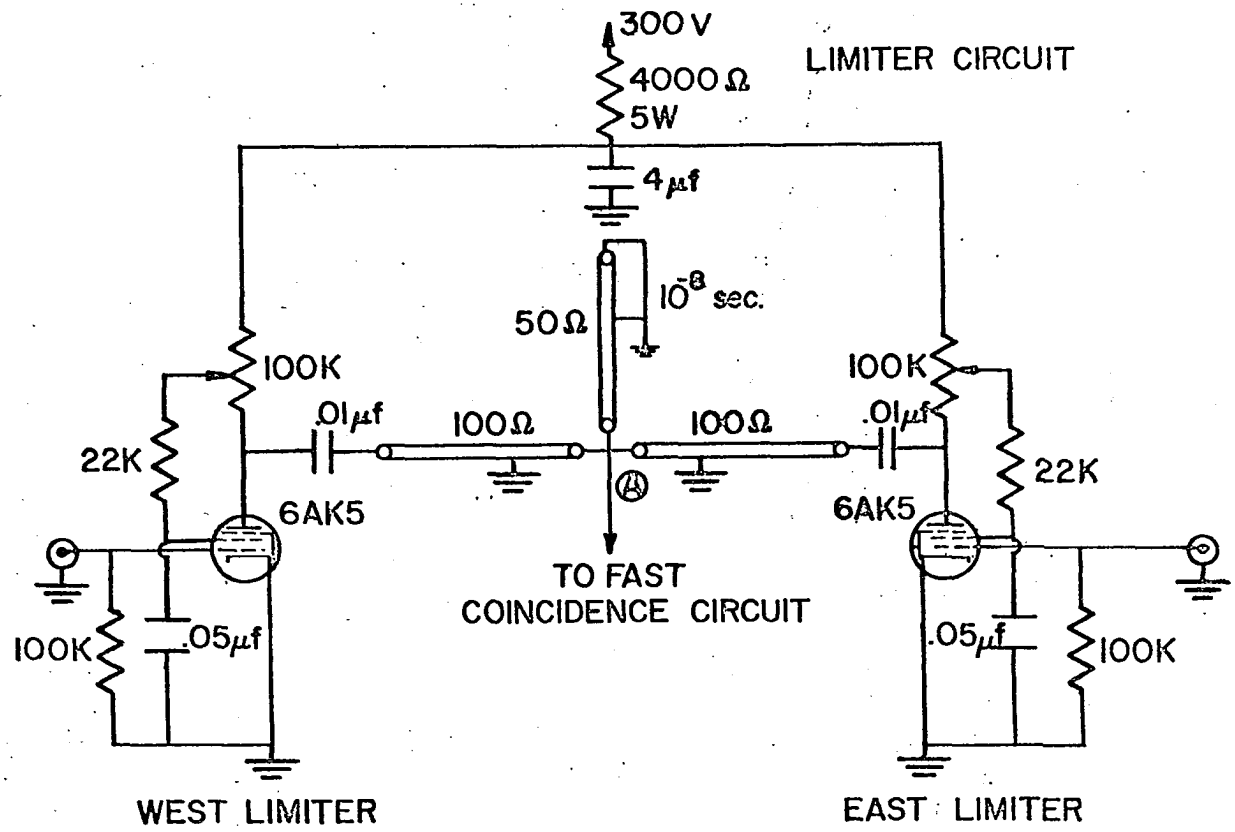


Figure 4. Diagram of the limiter circuit

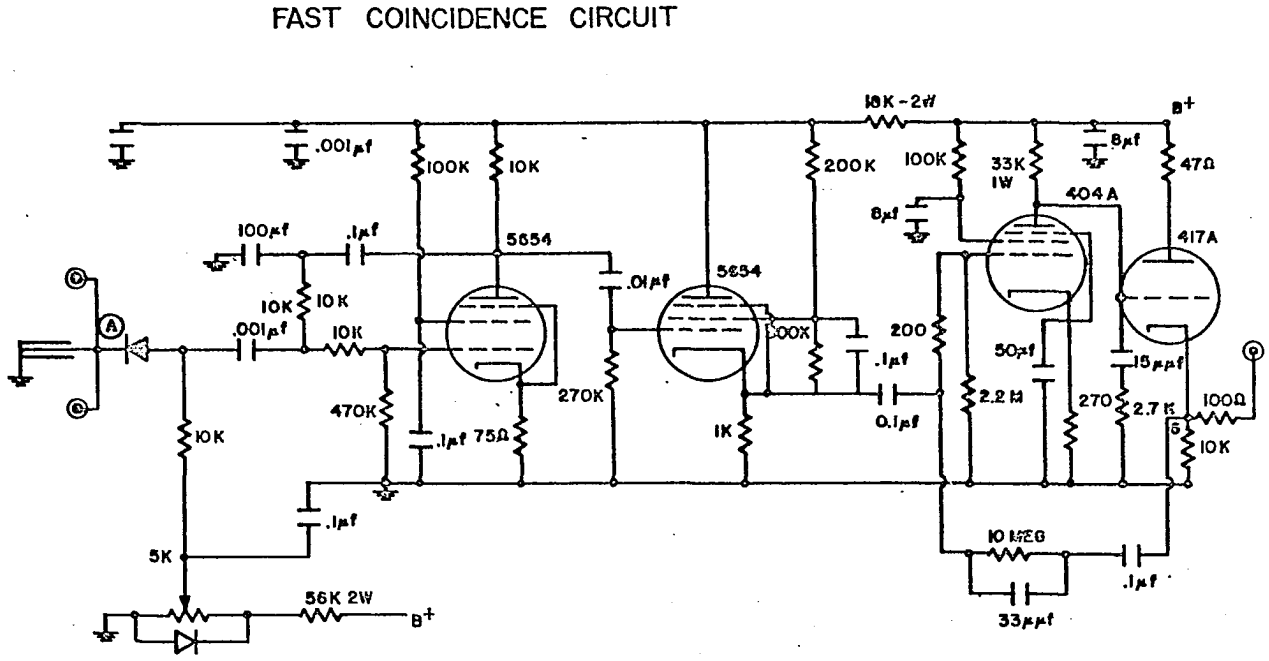


Figure 5. Diagram of the fast coincidence circuit

within 2μ sec. These coincidences corresponded to the .511 mev gamma rays due to positron annihilation with electrons. The coincidences were fed into a Control Measurement Corporation 704B printing scaler and printed out by a Control Measurement Corporation 400CT data printer at the end of each cycle. The cycle of the machine was controlled by a Programmer constructed by the electronics work shop in the Physics Department. The programmer was capable of counting for a preset time, after which it would signal the scalers to print out, reset the scalers, advance the arm ½ milliradian, and then begin counting again. The time spent counting in each position was 200 seconds so that counting over the full angular range, generally twelve milliradians, took about three hours. For this reason many sweeps were required to obtain a single positron annihilation curve. However, the effects due to drifts in the electronics and the error due to source decay were minimized.

## Sample Preparation

Fig. 6 shows a diagram of the furnace used in growing the single crystals of the rare earth metals and the rare earth alloy used in this experiment. The crystals were grown by means of a process developed by Nigh (38). The important features of the furnace are its two concentric tantalum cylinders, one 1 7/8 inches in diameter and 10 inches long and the other 2 1/4 inches in diameter and 9 3/8 inches long.

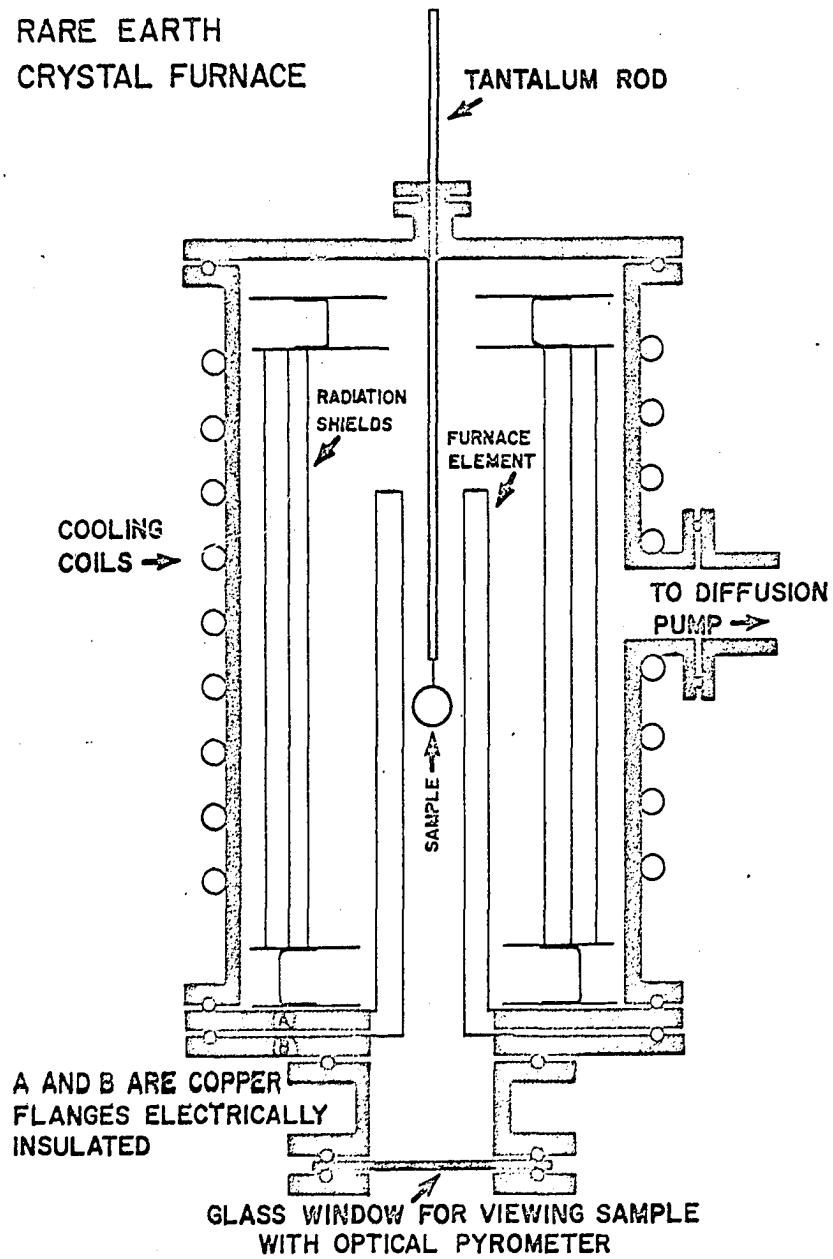


Figure 6. Diagram of the furnace used to grow the single crystals of the rare earths

The two cylinders were electrically connected by a ring at the top. With this construction,current, furnished by the secondary windings of a Westinghouse, type MTA, welding transformer and controlled by a Powerstat, type 1256D, Variac on the primary of the transformer, could be passed up the inner cylinder, through the ring, and back down the outer cylinder. As the tantalum cylinders were constructed out of 2 mil tantalum, the power dissipated by ohmic losses allowed temperatures up to 1600°C to be reached. The two noteworthy features of the furnace are its constant temperature region near the center of the cylinder (within $\pm$ 5° at 1250°C for a length of three inches) and a temperature gradient at the top (approximately 25°C/cm). It was found, experimentally, that some of the rare earths grow better in a gradient and some grow better in a constant temperature region.

The sample was suspended by a 30 mil tungsten wire in the high temperature region within the inner cylinder and viewed through a window at the bottom of the furnace. The button's temperature was monitored with an optical pyrometer. All annealing of the samples was carried out in a vacuum of $10^{-5}$ Torr or better. Table 1 shows the various times, pressures, and annealing temperatures of the buttons. These times and temperatures generally resulted in single crystal grains of 12 mm to 15 mm in diameter and 5 mm in thickness. Prior to annealing the samples were formed into arc melted buttons

of 35 mm diameter and 7 mm thickness. The pure rare earth metal buttons were first arc melted in one atmosphere of argon at 300 amps, turned over and then arc melted again at 300 amps. The alloy sample was turned over five times and arc melted at one atmosphere of argon and 300 amps each time. After annealing, the single crystals were cut from the button with a Sparcatron spark cutter and were oriented by means of a Laue backscattering x-ray camera. Finally, upon completion of the orientation, the crystals were spark cut into disks of approximately 10 mm in diameter and 3 mm in thickness and then electropolished.

# THEORY OF POSITRON ANNIHILATION IN METALS

## General Theory

The basic theory of positron annihilation in a metal was first developed by DeBenedetti, Cowan, Konneker, and Primakoff (8) by using the second order perturbation theory derivation of the annihilation probability based on the interaction of a Dirac electron with a quantized radiation field. This theory has been successfully applied to account for the shapes of the angular correlation curves, first by Berko *et al.* (20) and, more recently, by Loucks (39).

In the limiting case of the independent electron model the probability that an electron in the $\underline{k}^{th}$ state, with a wave function $\Psi_{\underline{k}}$, will annihilate with a positron, with a wave function $\Psi_{+}$, and result in two annihilation photons, with total momentum $\underline{p}$ lying in the range $d\underline{p}$, is given by (in atomic mass units with $\hbar = m = e = 1$)

$$A_{\underline{k}}(\underline{p})d\underline{p} = \frac{\alpha^3}{4\pi^2} \left| \int \Psi_{\underline{k}}(\underline{r})\, \Psi_{+}(\underline{r}) e^{-i\underline{p}\cdot\underline{r}}\, d\underline{r} \right|^2 d\underline{p} \qquad (1)$$

where $\alpha$ is the fine structure constant. The total rate of annihilation, $A(\underline{p})$, in the momentum range $d\underline{p}$ is given by summing over all possible electrons, or all possible states which are available for annihilation.

$$A(\underline{p})d\underline{p} = \sum_{\underline{k}} A_{\underline{k}}(\underline{p})d\underline{p} \qquad (2)$$

The rate of coincidences occurring at any angle, $N(\theta)$, is given by integrating the probability rate over the experimentally observable momenta range of the photon pairs which are able to enter the defining slits.

$$N(\theta)d\theta = \left(\int A(\underline{p})dp_x dp_y\right)dp_z \qquad (3)$$

This last equation predicts a result which can be measured experimentally. The correlation between the measurements and the results predicted by Equation 3 determines the validity of the independent particle model. However, before theoretically evaluating this equation, three things must be determined: the limits of the integrand; the wave functions of the electrons; and the wave function of the positron.

The first of these three, the limits, are determined by the range of momentum which the electron can assume. This range of momentum varies for the type of experimental measurements that one is interested in predicting.

The principal means of measuring $N(\theta)$ is the linear slit arrangement, a diagram of which is shown in Figure 2. In this arrangement the positron source and sample are stationary, and placed midway between two linear slits. Instruments, capable of measuring the coincidence of two gamma rays from the positrons annihilating with electrons in the sample, are placed behind the slits. By placing one of the slit-counter arrangements on a movable arm, one can determine the coincidence rate as a function of the angle between the photon

trajectories. As it will be shown in discussing the free electron model, a necessary condition for two photons to enter the slits is $p_z = mc\theta = c\theta$. In practice the slits are made long enough to describe an angular deviation in the vertical plane capable of accounting for the central width of the angular correlation curve. Thus, the experimental rate of coincidences observed at any angle, $\theta$, is proportional to

$$N(\theta)d\theta = \left(\int_{-\infty}^{\infty} dp_x \int_{-\infty}^{\infty} dp_y \, A(p_x, p_y, mc\theta)\right) dp_z \qquad (4)$$

The final step in theoretically calculating a numerical value for $N(\theta)$ is to determine the wave functions of the annihilating positrons and the electrons in a particular metal.

## Free Electron Gas

A very straightforward illustrative example of Equation 1 is to consider the angular correlations of ground state positrons annihilating with electrons in a free electron gas.

Suppose that two photons having momentum $\underline{p}_1$ and $\underline{p}_2$, as shown in Figure 7, are the result of a ground state positron annihilating a free electron. Then conservation of momentum requires

$$(p_2 - p_1)\cos\frac{\theta}{2} = p\cos\phi$$

$$(p_1 + p_2)\sin\frac{\theta}{2} = p\sin\phi = p_z$$

The relatively small kinetic energy of the electron can be neglected in conserving the mass-energy:

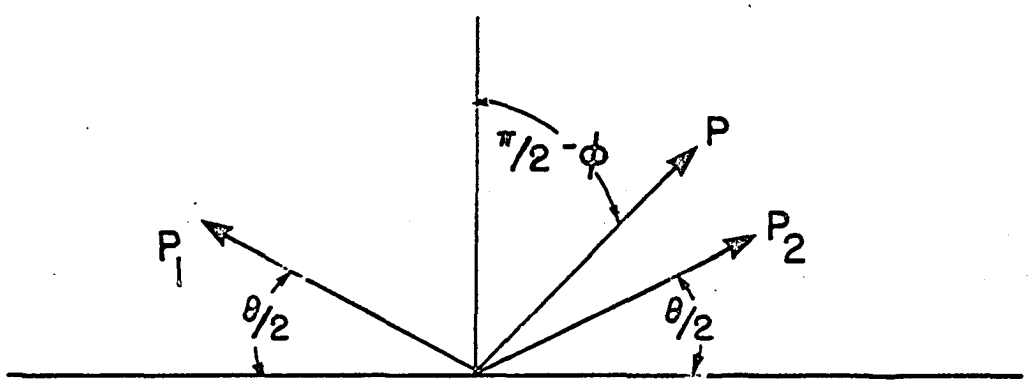


Figure 7. The momenta of the annihilation photons

$$c(p_1 + p_2) = 2mc^2$$

where c is the velocity of light and m is the mass of the interacting electron. Combining these three equations yields

$$\frac{p_z}{2mc} = \sin\frac{\theta}{2} \simeq \frac{\theta}{2} .$$

Thus, the $p_z$ component of momentum is proportional to the angle through which the annihilation gamma rays deviate from collinearity.

In the free electron model the wave functions of the electrons are plane waves and are given by

$$\Psi_{\underline{k}}(\underline{r}) = \frac{e^{i\underline{k}\cdot\underline{r}}}{\Omega^{\frac{1}{2}}}$$

where $\Omega$ is the volume of space in which the electrons are confined and $\underline{k}$ is the wave number of the electron.

The positron, being in the ground state, has zero wave number, and hence its wave function is given by

$$\Psi_{+}(\underline{r}) = \frac{e^{i0\cdot\underline{r}}}{\Omega^{\frac{1}{2}}} = \frac{1}{\Omega^{\frac{1}{2}}} .$$

With these two wavefunctions Equation 1 becomes

$$A_{\underline{k}}(\underline{p})d\underline{p} = \frac{\alpha^3}{4\pi^2} \left| \int \frac{e^{i\underline{k}\cdot\underline{r}}\ 1\ e^{-i\underline{p}\cdot\underline{r}}}{\Omega} d\underline{r} \right|^2 d\underline{p}$$

$$= \left[ \frac{\alpha^3}{4\pi^2} (2\pi)^3 \frac{1}{\Omega^2} \delta(\underline{k}-\underline{p}) \int e^{i(\underline{p}-\underline{k})\cdot\underline{r}} d\underline{r} \right] d\underline{p}$$

$$= \left[ \frac{2\pi\alpha^3}{\Omega} \delta(\underline{k}-\underline{p}) \int \frac{d\underline{r}}{\Omega} \right] d\underline{p}$$

$$= \frac{2\pi\alpha^3}{\Omega} \delta(\underline{k}-\underline{p}) \; d\underline{p}$$

Thus, for a linear slit arrangement the rate of observable coincidences is

$$N(\theta)d\theta = \frac{2\pi\alpha^3}{\Omega} \left[ \int_{-\infty}^{\infty} dp_x \int_{-\infty}^{\infty} dp_y \sum_k \delta(\underline{k}-\underline{p}) \right] dp_z$$

Since $p_z = c\theta$, this equation can be rewritten as

$$N(\theta) = \frac{2\pi\alpha^3 c}{\Omega} \int_{-\infty}^{\infty} dp_x \int_{-\infty}^{\infty} dp_y \sum_k \delta(k_x-p_x) \, \delta(k_y-p_y) \, \delta(k_z-p_z)$$

$$N(\theta) = \frac{2\pi\alpha^3 c}{\Omega} \sum_k \delta(k_z-p_z)$$

From this equation it is apparent that $N(\theta)$ is proportional to the number of occupied electron states with $k_z = c\theta$. The occupied states are those states whose phase space volume is enclosed by the Fermi surface. In the case of the free electron gas the Fermi surface is a sphere and from Figure 8 it is clear that the number of occupied states with $p_z = k_z = c\theta$ is proportional to the area of a slice through the Fermi surface and perpendicular to the $k_z$ axis. From this same figure the area of such a slice is given by

$$A_{F.S.} = k_F^2 - k_z^2$$

or,

$$A_{F.S.} = k_F^2 - (c\theta)^2 \; .$$

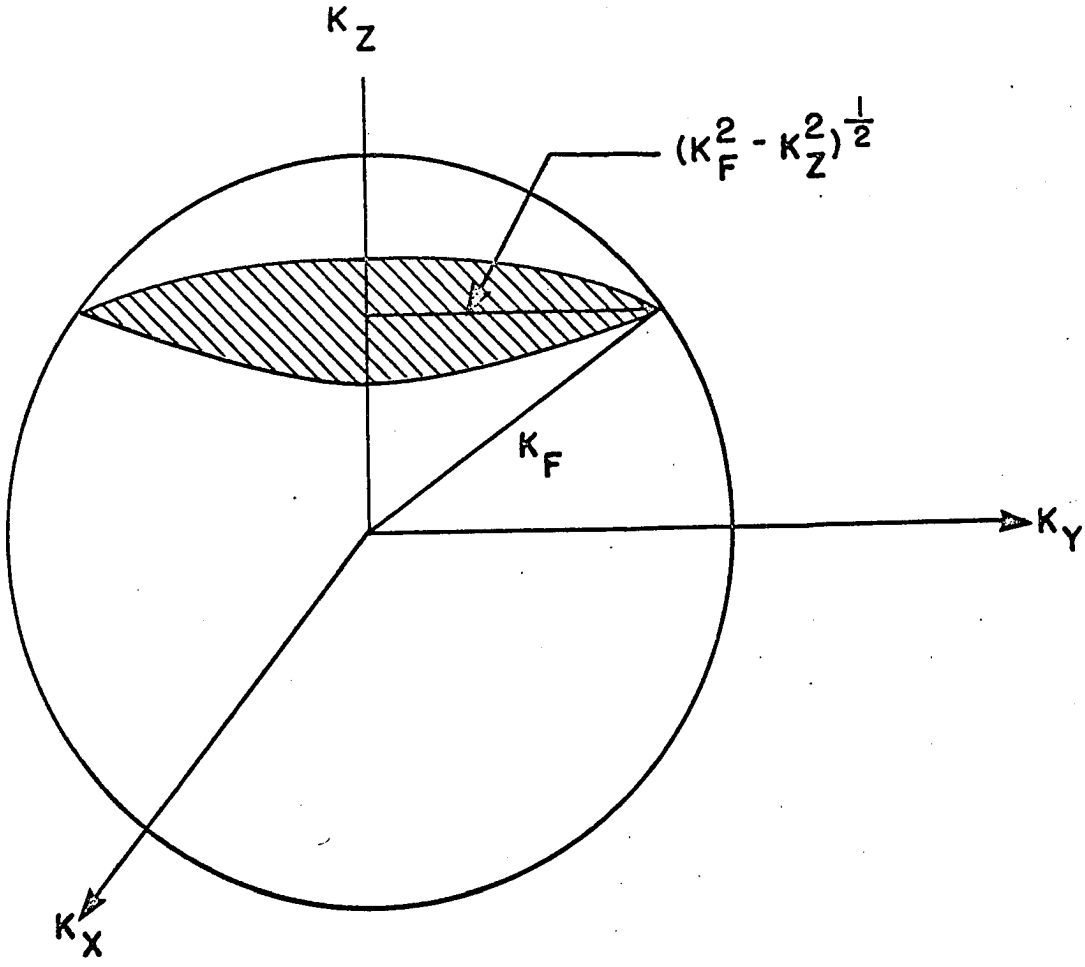


Figure 8. Variation of Fermi surface area with $k_z$ for the free electron gas

Therefore, the rate of observable coincidences is given by

$$N(\theta) \sim k_F^2 - (c\theta)^2$$

or,

$$N(\theta) \sim c^2(\theta_F^2 - \theta^2)$$

where $\theta_F$ is defined by

$$\theta_F = \frac{k_F}{c} .$$

The observable coincidence rate for a free electron gas is just a parabola centered at $\theta = 0$ and falling to zero at the value $\theta = \frac{k_F}{c}$.

Real Metal

In the case of a real metal, the wave function of both the positron and the electrons are described by Bloch functions,

$$\Psi_{\underline{k}}(\underline{r}) = \chi_k(\underline{r})e^{i\underline{k}\cdot\underline{r}}$$

$$\Psi_+(\underline{r}) = \chi_+(\underline{r})e^{i\underline{l}\cdot\underline{r}} .$$

In this formulation the wave functions of the electrons and positron are plane waves, $e^{i\underline{k}\cdot\underline{r}}$ and $e^{i\underline{l}\cdot\underline{r}}$, modulated by functions, $\chi_k(\underline{r})$ and $\chi_+(\underline{r})$, having the periodicity of the lattice. With the assumption that the positron is in its ground state, the wave function can be written as

$$\Psi_+(\underline{r}) = \chi_+(\underline{r}) .$$

Equation 1 thus becomes

$$A_k(\underline{p})d\underline{p} = \frac{\alpha^3}{4\pi^2} \left| \int \chi_k(\underline{r})e^{i\underline{k}\cdot\underline{r}} \chi_+(\underline{r})e^{-i\underline{p}\cdot\underline{r}} d\underline{r} \right|^2 d\underline{p} .$$

This equation can be simplified by defining $\underline{r} = \underline{g} + \underline{r}'$ where $\underline{r}'$ is confined to a unit cell and $\underline{g}$ is an arbitrary lattice vector. Hence, the expression can be rewritten as an integral over a unit cell, summed over all unit cells throughout the lattice. Since the $\chi$'s have the periodicity of the lattice

$$\chi_k(\underline{r}' + \underline{g}) = \chi_k(\underline{r}')$$

$$\chi_+(\underline{r}' + \underline{g}) = \chi_+(\underline{r}')$$

and Equation 1 reduces to

$$A_{\underline{k}}(\underline{p})d\underline{p} = |F(\underline{p},\underline{k})|^2 d\underline{p}$$

where

$$F(p,k) = \sum_{\text{crystal}} e^{i(\underline{k}-\underline{p})\cdot\underline{g}} \int e^{i(\underline{k}-\underline{p})\cdot\underline{r}'} \chi_k(\underline{r}')\,\chi_+(\underline{r}')d\underline{r}'$$

$$= \sum_{\underline{g}_n} A_{\underline{g}_n}\,\delta(\underline{k} + \underline{g}_n - \underline{p})$$

if $\underline{g}_n = \underline{k} - \underline{p}$.

In practice the ground state positron wave function goes to zero in the core region and has a single, flat maximum outside the core region. One such positron wave function may be seen in Figure 9. This behavior is due to the repulsive nature of the positive core. Since the wave function of the positron is largest outside the core, its probability of being found there, given by the amplitude of the wave function squared, is greatest. Consequently, the conduction electrons

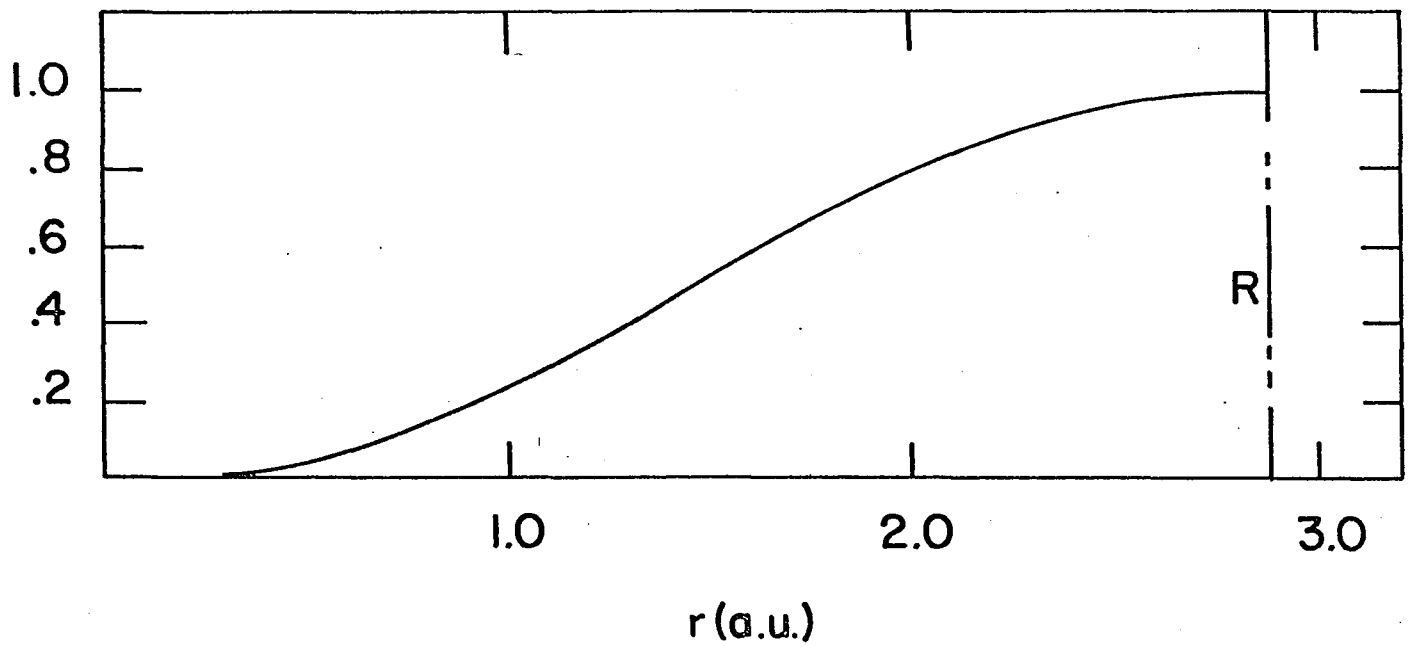


Figure 9. A ground state positron wave function calculated by the Wigner-Seitz method (39)

give a much larger contribution than the individual core electrons and for simple metals, in which the conduction electron wave functions are like plane waves outside the cores, the first term of $A_{gn}$ dominates. However, for transition metals, several $A_{gn}$ may contribute significantly.

# DISCUSSION

## Comparison of Theory and Experiment for Yttrium

As the theoretical calculation of the angular correlation curves involves the square of the overlap integral between the electron, positron, and photon wave functions, it should provide a sensitive test of both the wave functions and the independent particle model. The only attempt to make such a calculation of an angular correlation curve for a rare earth metal was made recently by T. L. Loucks, who calculated the theoretical angular correlation curve for yttrium (39). The atomic configuration for yttrium, $4d5s^2$, is very similar to the $5d6s^2$ atomic configuration of the heavy 4f rare earth metals. Yttrium is not, however, complicated by either magnetic or relativistic effects.

Loucks' theoretical study of the electronic structure of yttrium was based on an augmented plane wave (APW) calculation using the original method proposed by Slater (40). The angular distribution of the positron annihilation radiation was calculated by using 22 reciprocal lattice vectors in the expansion of the electron wave function and the Wigner-Seitz model for the positron wave function.

In the APW method the electronic wave functions are written

$$\chi(\underline{k},r) = \sum_{\underline{g}} \xi(\underline{g},\underline{k})\ \mathrm{APW}(\underline{k} + \underline{g})$$

where

$$APW(\underline{k}) = e^{i\underline{k}\cdot\underline{r}}$$

outside the APW sphere , and

$$APW(\underline{k}) = 4\pi\, e^{i\underline{k}\cdot(\underline{r}_\nu + \underline{\tau})} \sum_{lm} i^l j_l(kR)\, \frac{U_l(\rho)}{U_l(R)}\, Y^*_{lm}(\underline{k}) Y_{lm}(\rho)$$

inside the sphere. Here $\underline{r}_\nu$ is the lattice vector of the $\nu^{th}$ cell, $\underline{\tau}$ is a vector pointing to the center of the APW sphere with radius R, $\rho$ is the radial coordinate centered on the APW sphere, $U_l(\rho)$ is the solution of the radial Schrodinger equation in the spherically symmetric potential, and $\xi(\underline{g},\underline{k})$ are the expansion coefficients determined from the variational principle. Figure 10 shows this coordinate system.

Since the APW's are based on a spherical muffin-tin potential, the positron wave function is approximated by constructing a muffin-tin potential using the same APW sphere as for the electrons. The muffin-tin potentials which were used in Loucks' calculation are shown in Figure 11.

Since the positron is assumed to be in its ground state, the wave function outside the spherical region is taken to be constant and inside it is the ground state solution to the radial Schrodinger equation (regular at the origin) subject to the boundary conditions at the edge of the sphere:

$$\Psi_+(R) = 1$$

and

$$\Psi'_+(R) = 0 .$$

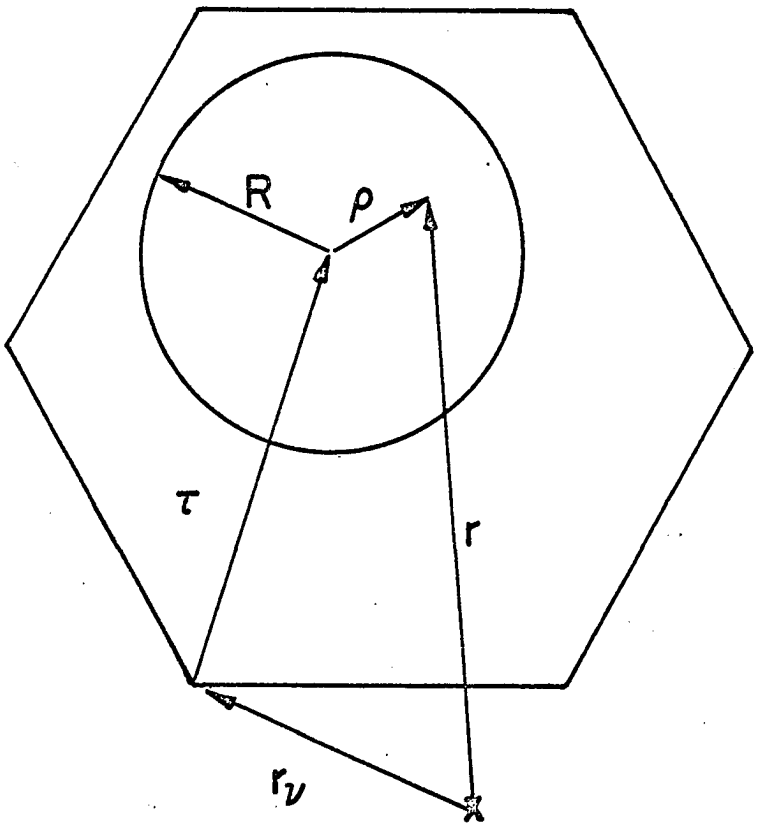


Figure 10. Coordinate system used in the APW calculation (39)

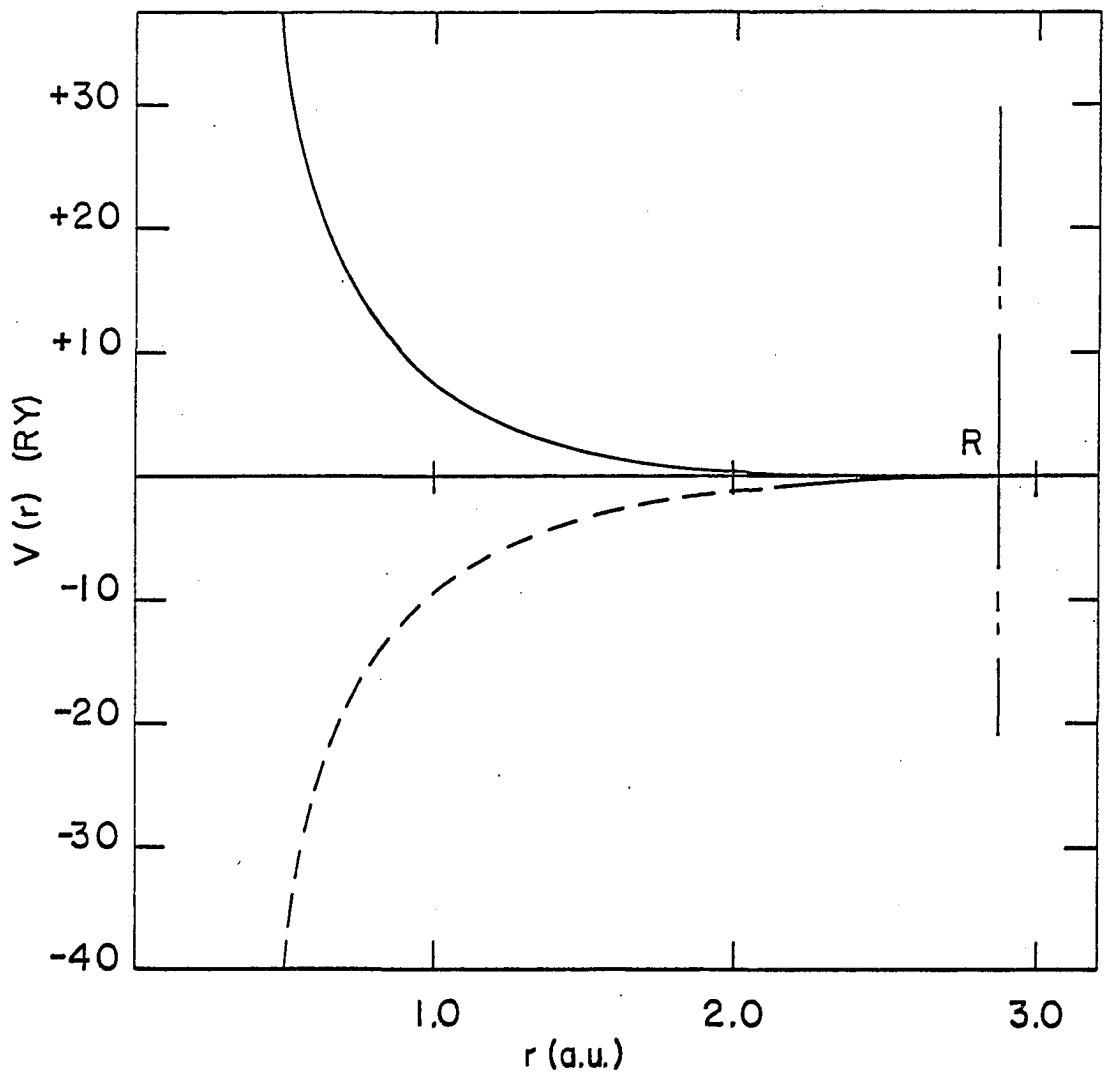


Figure 11. The muffin-tin potentials (39)

Figure 9 shows a positron wave function obtained in this manner. The wave function is what one might expect of the wave function for a ground state positron in a lattice potential. It has only one maximum and one minimum. The maximum lies outside the APW sphere and, since the probability of being found at some location is proportional to the square of the wave function, it is most probable that the positron will be there. The minimum lies at the origin, on the lattice site, which shows that because of Coulomb repulsion the positron's probability of being found within the APW sphere decreases with decreasing distance from the origin and is zero at the lattice site.

In calculating

$$\left| \int \Psi_{+}(r) \Psi_{\underline{K}}(r) e^{-i\underline{p}\cdot\underline{r}} \, d\underline{r} \right|^2$$

and obtaining a theoretical angular correlation curve for yttrium, Loucks considered only the annihilations with s and d electrons and necessarily neglected electron-positron correlation. The experimental results of the angular correlation curve for a c-axis (0001) crystal of yttrium are compared with his theoretical results in Figure 12. (The theoretical curve contains a resolution correction due to the slit width of the experimental apparatus.) There is good agreement on the two main features of the curves. Both curves for small momenta drop sharply below the free-electron parabola and both curves exhibit a hump at about 3mrad. The hump has its origin

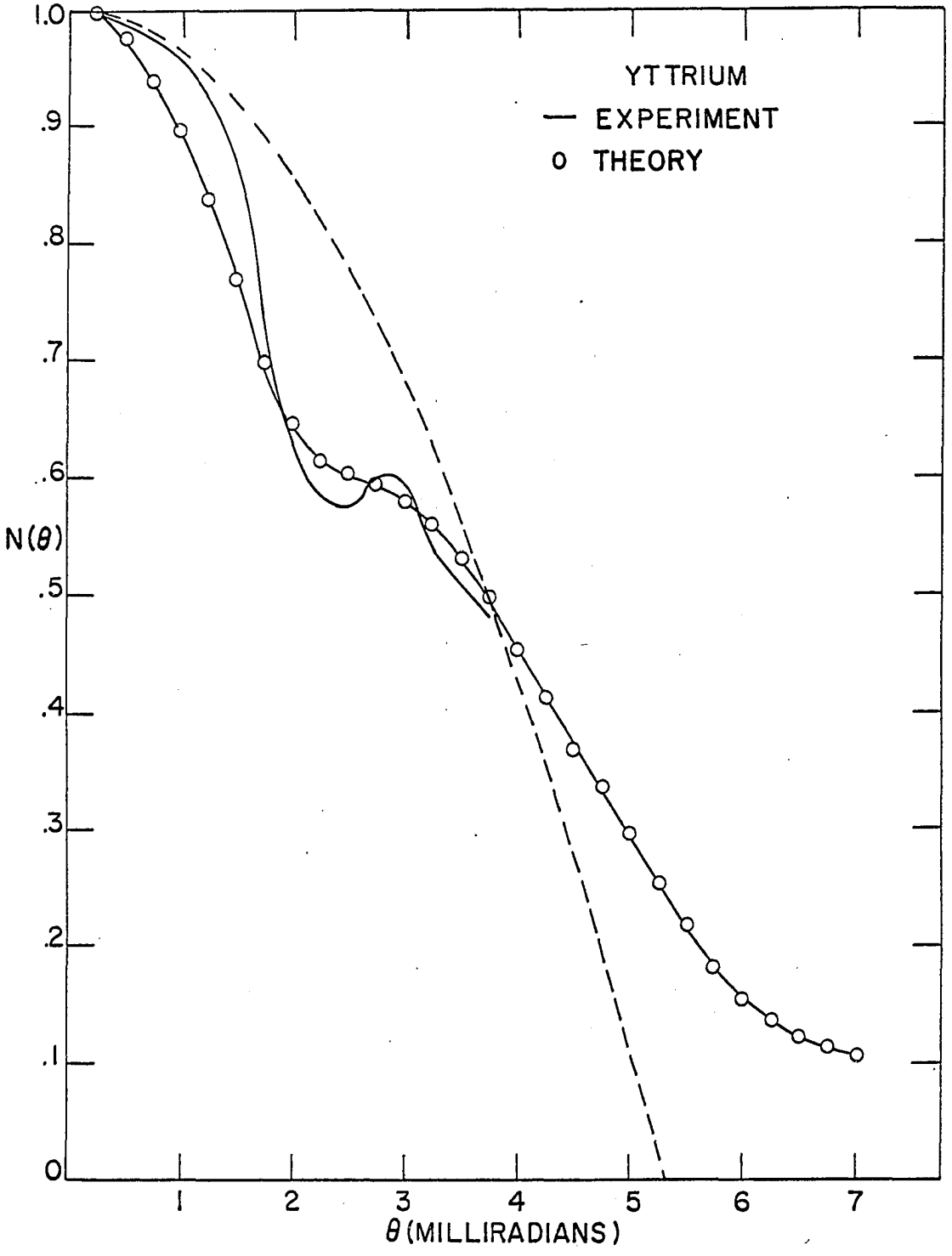


Figure 12. The theoretical and experimental angular correlation curves of a c-axis(0001) yttrium crystal

in particular features of the Fermi surface. One can obtain a qualitative idea of the relation between the Fermi surface and the angular correlation curve as follows: in the independent particle model $N(p_z) = N(\theta)$ is calculated by summing matrix elements of the form

$$\left|\int \psi_+(\underline{r})\psi_{\underline{k}}(\underline{r})e^{-i\underline{p}\cdot\underline{r}}\, d\underline{r}\right|^2$$

over all occupied states in the appropriate slice through the Brillouin zone. One may write

$$N(p_z) = A(p_z)F(p_z)$$

where $A(p_z)$ is the number of occupied states in a slice and satisfies the relation

$$A(p_z + g_z) = A(p_z)$$

while $F(p_z)$ is a form factor which varies smoothly with $p_z$ and for conduction electrons generally decreases rapidly for values of $p_z$ lying outside the primitive Brillouin zone. If the wavefunctions were all free electron wavefunctions corresponding to the $\underline{k}$ value within the primitive zone for instance, $F(p_z)$ would be constant for $p_z$ within the zone and zero outside. In Figure 13 we have plotted $A(p_z)$ and $F(p_z)$ deduced from the calculations of Loucks (39), shown in Figures 14, 15 and 16. It is clear from these functions that the rapid drop at low $p_z$ is primarily due to the rapid drop in occupied states as the zone boundary is approached, while the maximum in the curve reflects the combined effect of the rapid increase of $A(p_z)$ with the rapid decrease of $F(p_z)$. The rapid

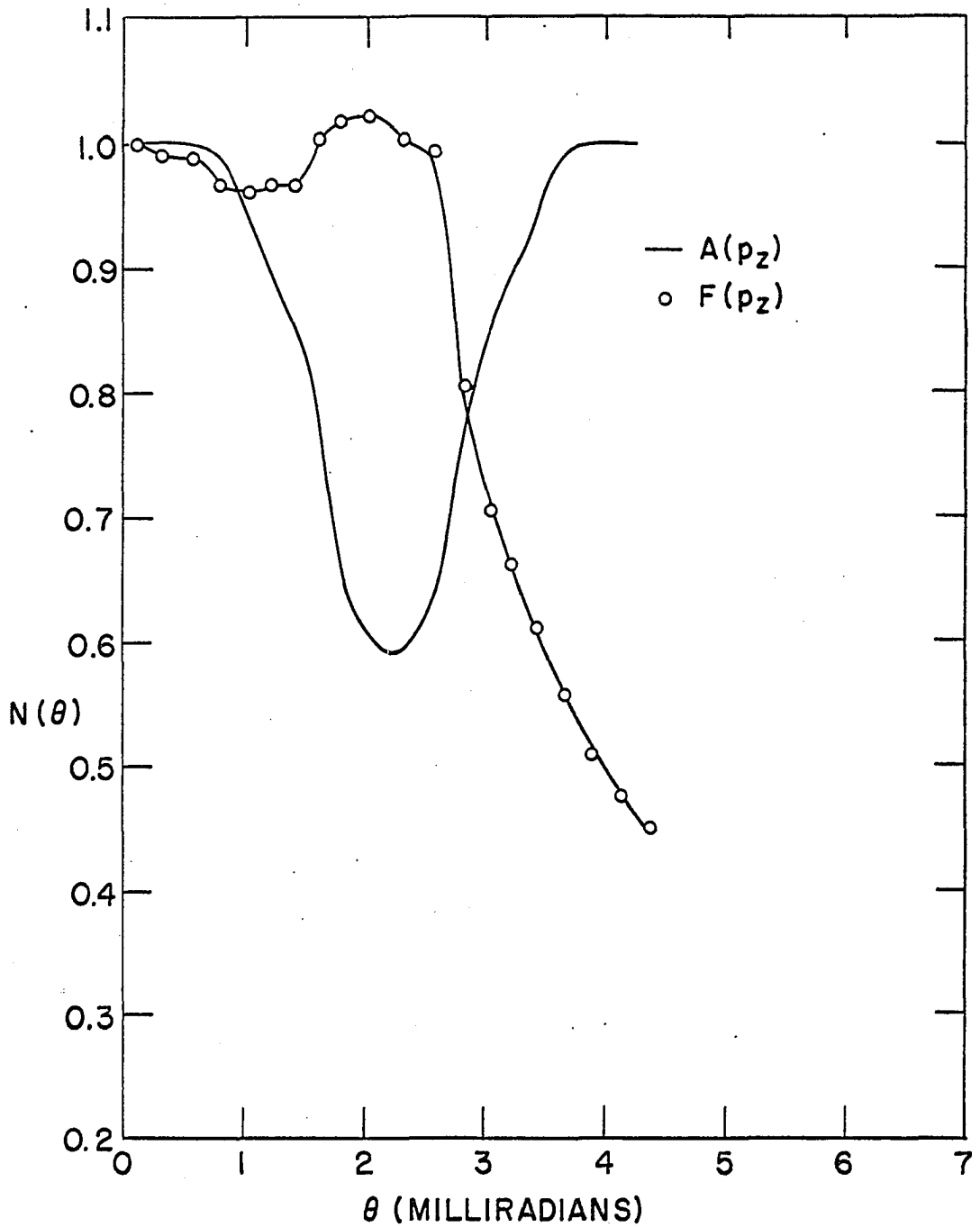


Figure 13. The number of occupied states, $A(p_z)$, and the form factor, $F(p_z)$, plotted against angle

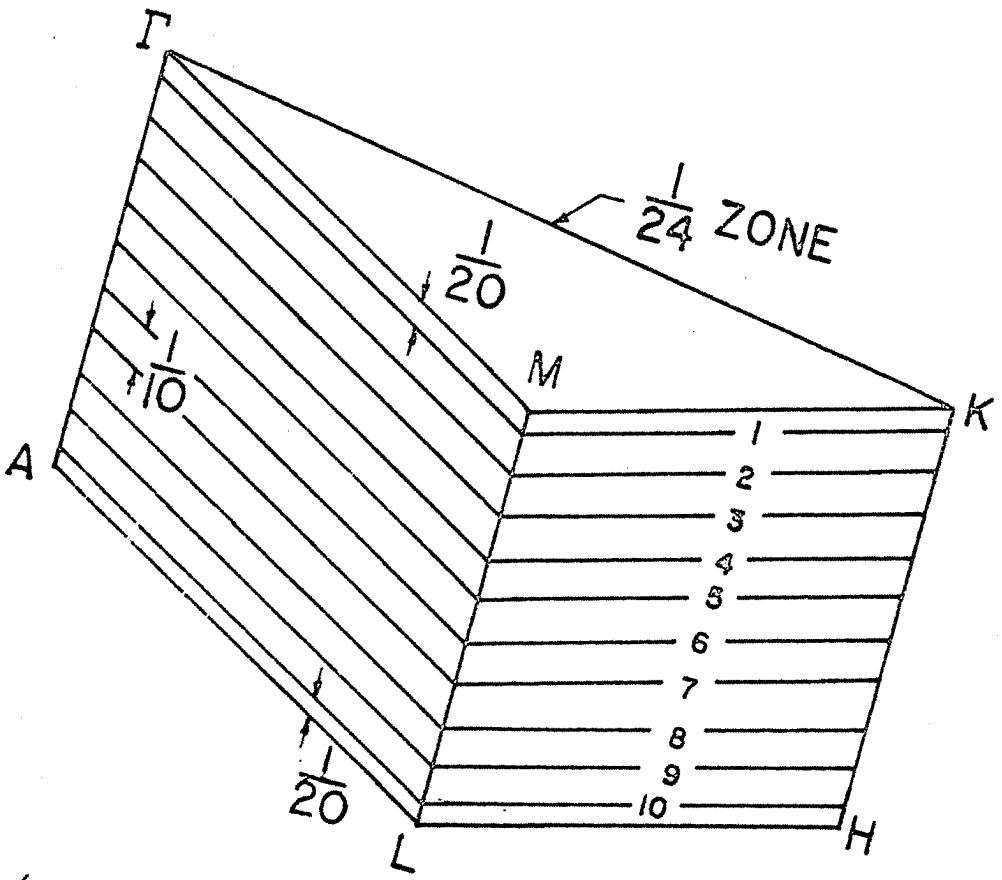


Figure 14. 1/24 of a Brillouin zone showing the positions of the ten slices of the Fermi surface (39)

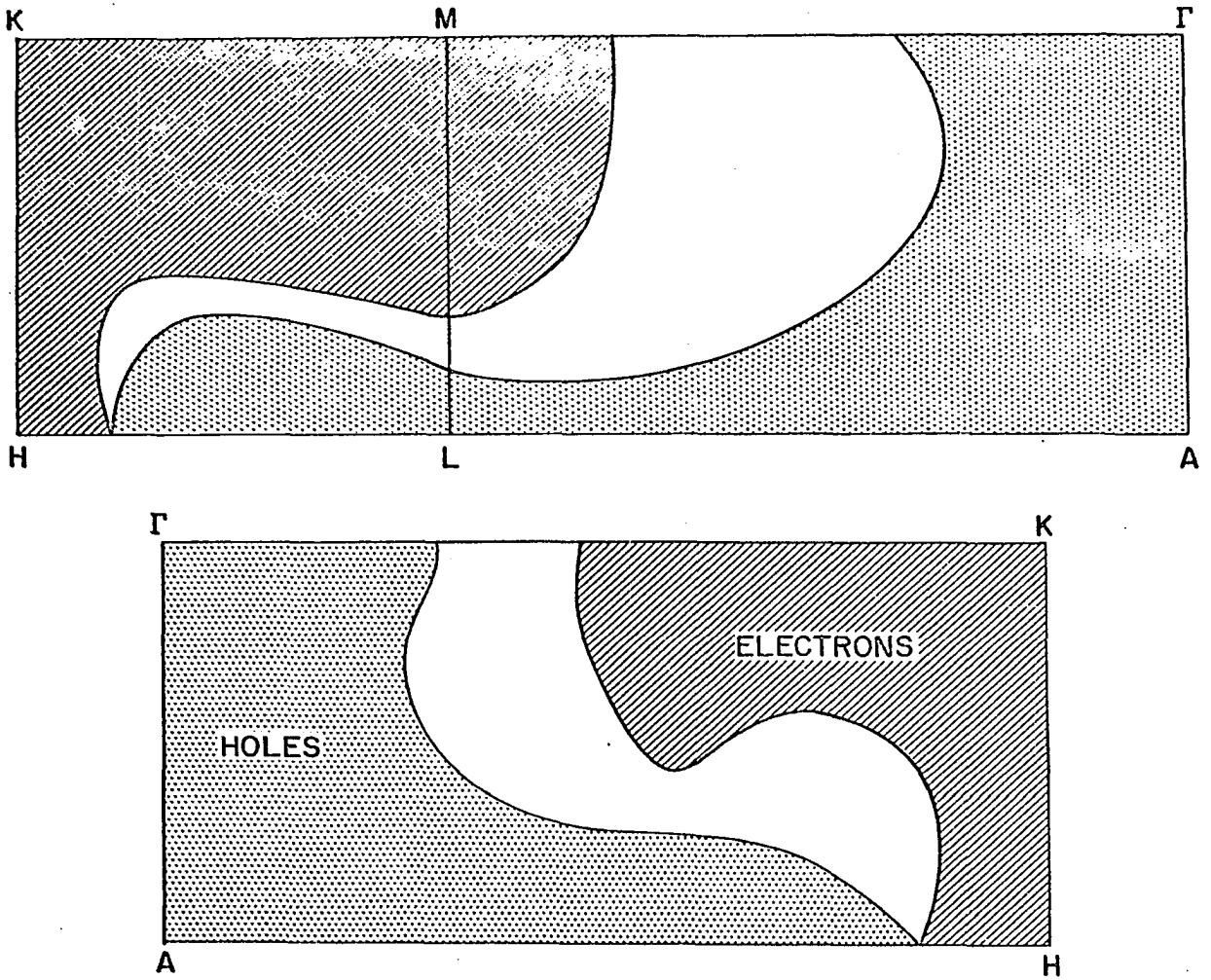


Figure 15. Intersections of the Fermi surface of yttrium with the faces of the 1/24 Brillouin zone (39)

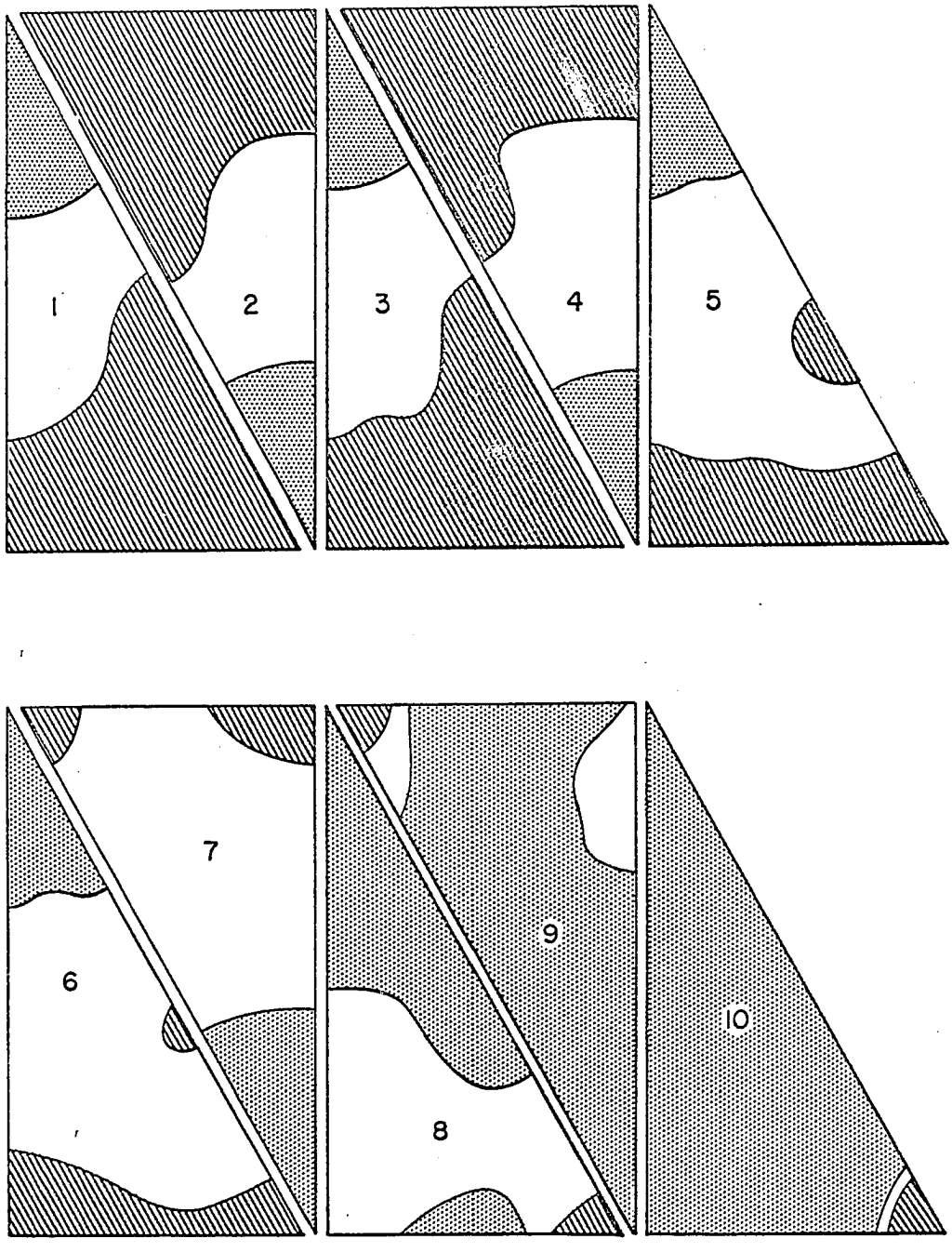


Figure 16. Intersections of the Fermi surface with the planes shown in Figure 14 (39)

change of $A(p_z)$ with $p_z$ is in turn a manifestation of the flat regions of the Fermi surface normal to the c-axis. We may say qualitatively, therefore, that the rapid decrease and hump are reflections of the flatness of the Fermi surface in the c-direction.

Figure 17 shows the experimental angular correlation curve for a b-axis $(10\bar{1}0)$ crystal of yttrium compared to the c-axis (0001) results.

For comparison the two curves are normalized so that their areas are the same. This assumes that an equal number of electrons are annihilated in any direction for the same momentum region, 0 to 9 mrad., which is probably a good approximation. The b-axis angular correlation curve follows the free parabola curve for low momentum and exhibits no hump. From Figure 16 it can be seen that this is because there are no rapid changes in the number of electron states in slices through the Brillouin zone normal to the b-axis.

The experimental curve for the b-axis crystal, quite different from that for the c-axis crystal in the region 0 mrad. to 3.5 mrad., manifests the highly anisotropic nature of the Fermi surface of yttrium.

The qualitative agreement between the experimental results and the theoretical results shows that the independent electron model is not a bad first order approximation. Further, the Coulomb correlation does not, as it might first

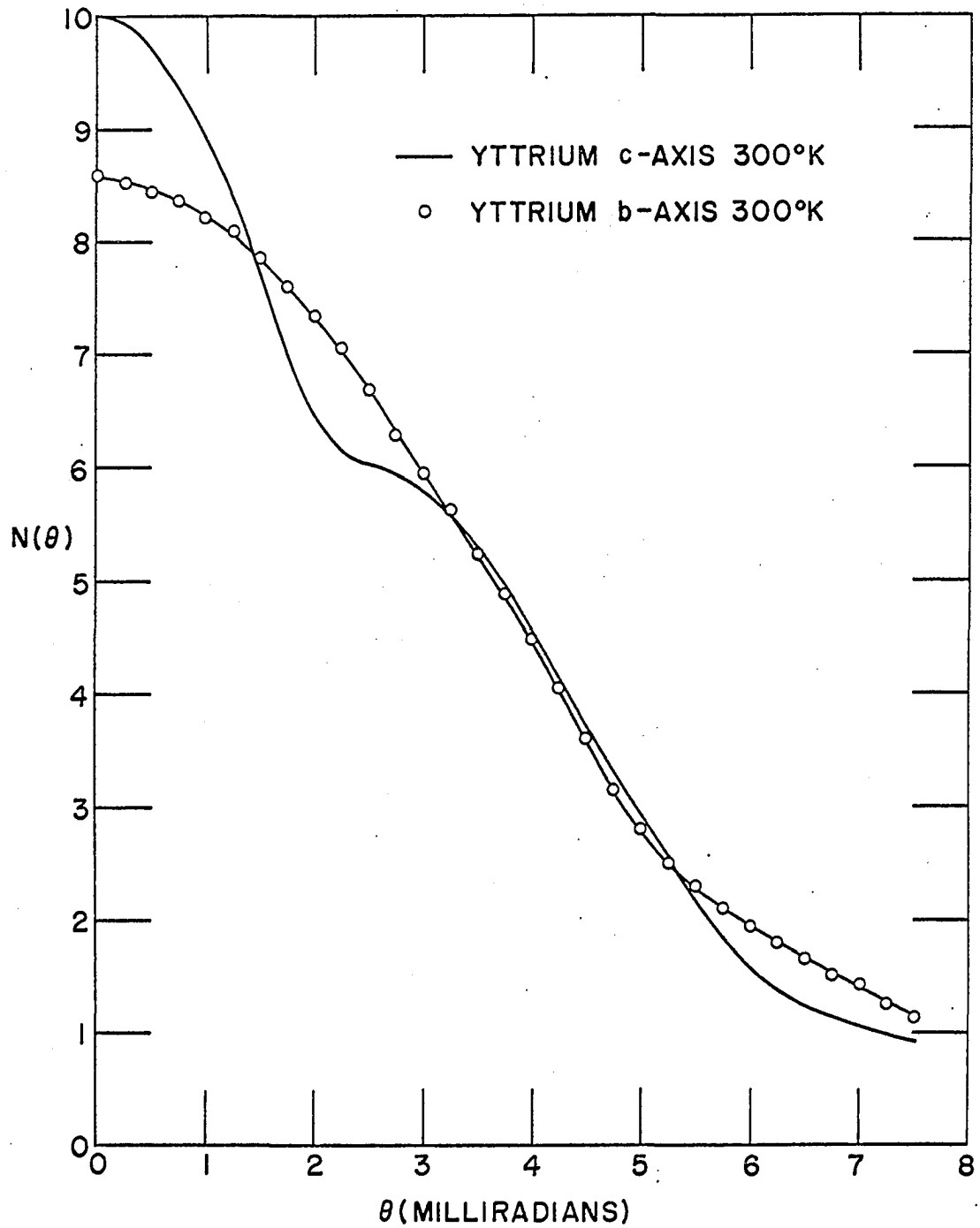


Figure 17. The experimental angular correlation curves of a b-axis (10$\bar{1}$0) and a c-axis (0001) yttrium crystal

be supposed, completely eliminate the hump; although it apparently suppresses some of the details of the curve. Finally, the qualitative agreement indicates that the theoretical band structure for this metal is at least qualitatively correct.

## Magnetic Effects

The electronic configuration of the rare earth metals, which were studied in this experiment, consists of three electrons with s-d character occupying the conduction band and a partially filled 4f shell. There are seven electrons in the 4f shell of gadolinium and for each unit increase in atomic number through ytterbium the number increases by one. These 4f electrons, describable by localized atomic-like Wannier functions, occupy bound states and have negligible direct interactions with the 4f electrons on neighboring sites. Because of this localization the 4f electrons contribute little to the angular correlation curves at room temperature, and, as might be expected, the s-d electrons give the major contributions to the annihilation process. However, when the 4f magnetic moments are ordered, as in the case of holmium at low temperatures, they can affect the angular correlation curves indirectly by modifying the conduction electron distribution.

The observed magnetic structure of holmium in zero magnetic field is shown in Figure 18. This element changes

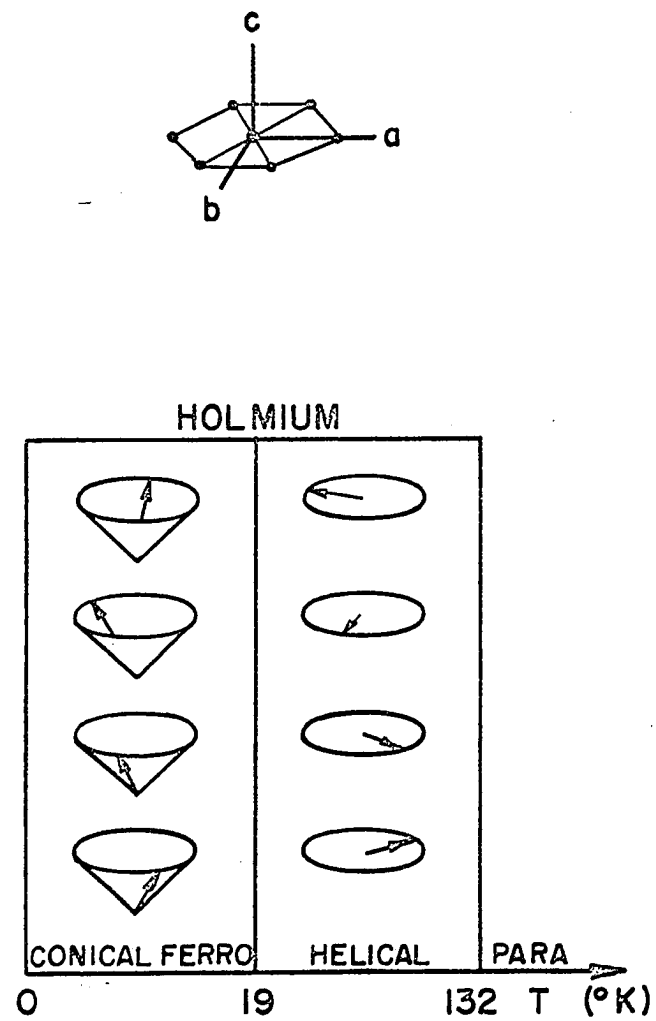


Figure 18. The magnetic structure of holmium in zero magnetic field

progressively from a paramagnetic structure at room temperature, to a helical, antiferromagnetic structure at 132°K, to a conical ferromagnetic structure at 19°K. In the helical structure the moments are perpendicular to the c-axis and are aligned ferromagnetically, but the direction of the moments turns through an angle from layer to layer. This ordering gives a spiral structure about the c-axis direction. The important feature of this spiral magnetic structure is that it repeats itself with a period which is generally incommensurable with that of the lattice. This magnetic super-lattice gives rise, in turn, to a magnetic Brillouin zone structure, and introduces extra planes of energy discontinuity in reciprocal space.

An example of an electron interacting with a periodic structure is provided by the energy gaps introduced at the Brillouin zone in the one dimensional nearly free electron model (41). As can be seen in Figure 19, there are energy gaps at the Brillouin zone given by $2|V_g|$, where $V_g$ is the Fourier component of the potential for the reciprocal lattice vector g. The dashed line represents the parabolic band that the electron would occupy in the absence of a potential. In three dimensions the energy gaps occur on planes in $\underline{k}$ space, and generally have the effect of modifying the electronic structure and distorting the Fermi surface (36,42).

In the magnetic case, the mechanism primarily responsible

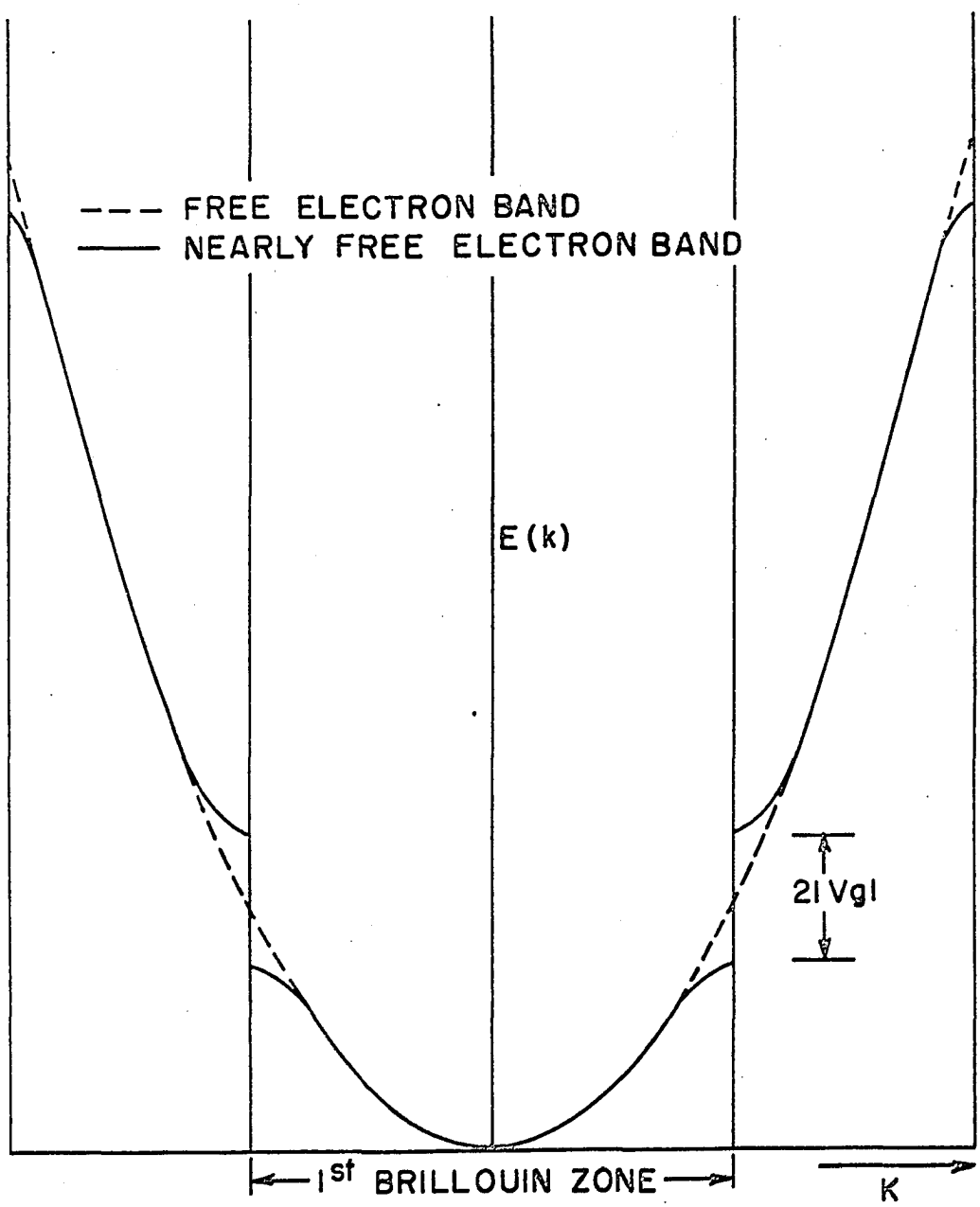


Figure 19. The energy of free and nearly free electrons in a one dimensional reciprocal lattice (41)

for the magnetic ordering is the indirect exchange interaction between the 4f electrons and the s-d conduction electrons (43). The exchange, in a particular approximation, is given for s-like electrons by

$$H = -2I(k,k')(g-1)\underline{s}\cdot\underline{J}$$

where I is an effective exchange integral, g the Landé factor for ionic moment $\underline{J}$, and $\underline{s}$ the conduction electron spin (44). In addition there are anisotropy fields which orient the moments relative to the crystal axis and in the particular case of holmium, this anisotropy energy tends to keep the moments in the basal plane. The exchange energy acts to cause the moments along the c-direction to spiral about the basal plane. Thus, in the c-direction the magnetic periodicity gives rise to energy gaps which cause a distortion of the Fermi surface.

The theoretical holmium Fermi surface is quite similar to that of yttrium and shows large, approximately flat electron and hole regions normal to the c-axis. These surfaces run parallel to each other over a large region when spin-orbit coupling is taken into account in a relativistic APW calculation. It has been recently proposed that their separation primarily determines the $\underline{Q}$ vector of the periodic magnetically ordered states, and that large parts of the surfaces are eliminated in magnetic ordering (45). As has been pointed out,

the electronic configurations of the two metals are quite similar with the exception that holmium has localized 4f electrons which give rise to its interesting magnetic properties. However, the two experimental angular correlation curves, shown in Figure 20 are very similar and this verifies, at least qualitatively, the similarity between the two Fermi surfaces. As a consequence of the flat electron and hole regions, the holmium curve shows the same hump as yttrium. The b-axis results are shown in Figure 21 and Figure 22 where they are compared to the yttrium b-axis results and the holmium c-axis results respectively. The fact that the c-axis curves and the b-axis curves of yttrium and holmium appear the same shows that the contribution of the 4f electrons to the angular correlation curve of holmium must be small and that most of the annihilations are, therefore, with the s and d electrons. The fact that the c-axis curve of holmium differs so radically from its b-axis curve and the free-electron parabola is a clear manifestation of the anisotropic nature of the holmium Fermi surface.

Figure 23 shows the angular correlation curve for the holmium c-axis crystal at 60°K compared to the angular correlation curve for the same crystal at room temperature. The angular correlation curves of the holmium in the spiral phase differs from its angular correlation curve in the paramagnetic phase in that the hump has disappeared. This is because the

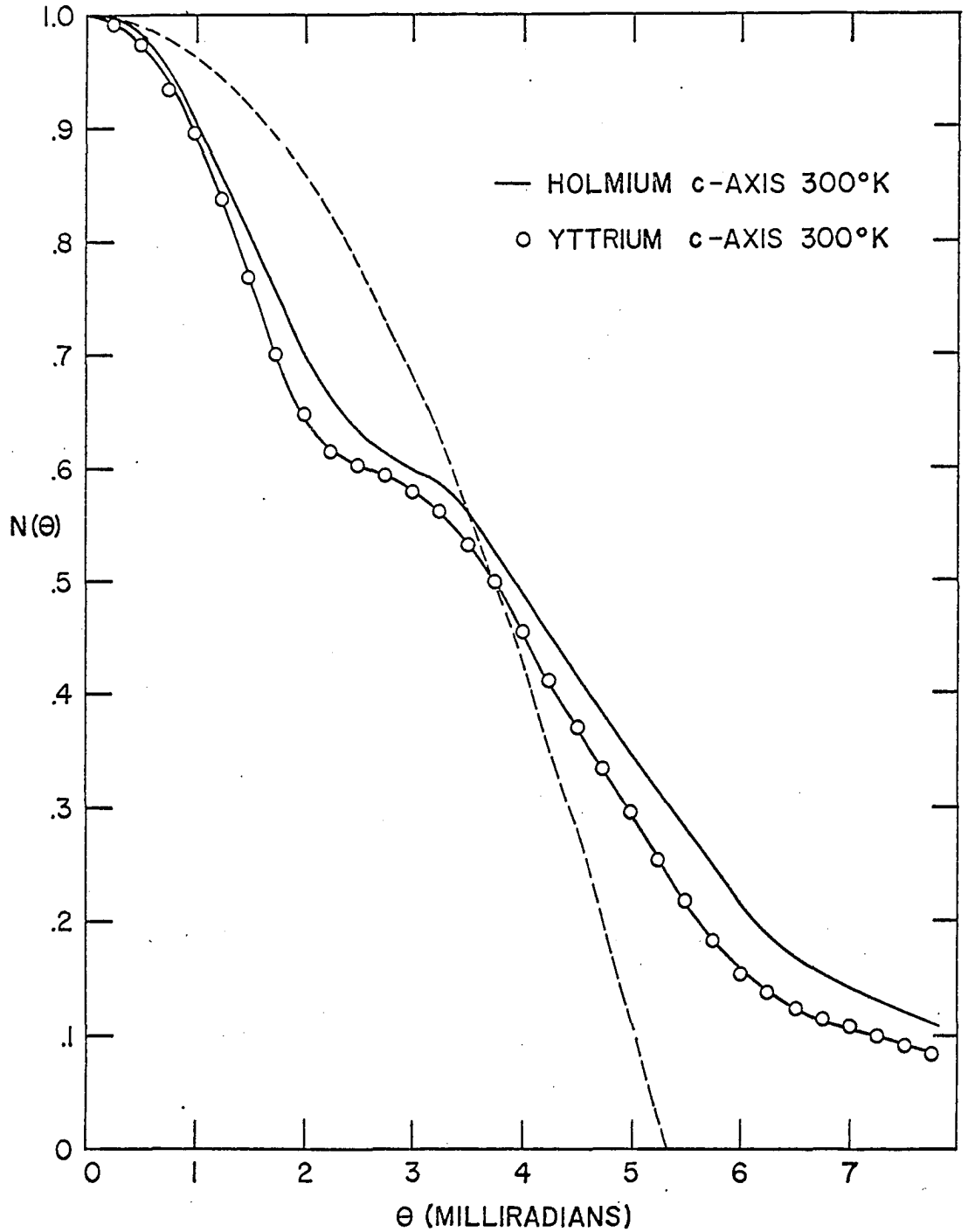


Figure 20. The experimental angular correlation curves of a c-axis (0001) holmium crystal and a c-axis yttrium crystal

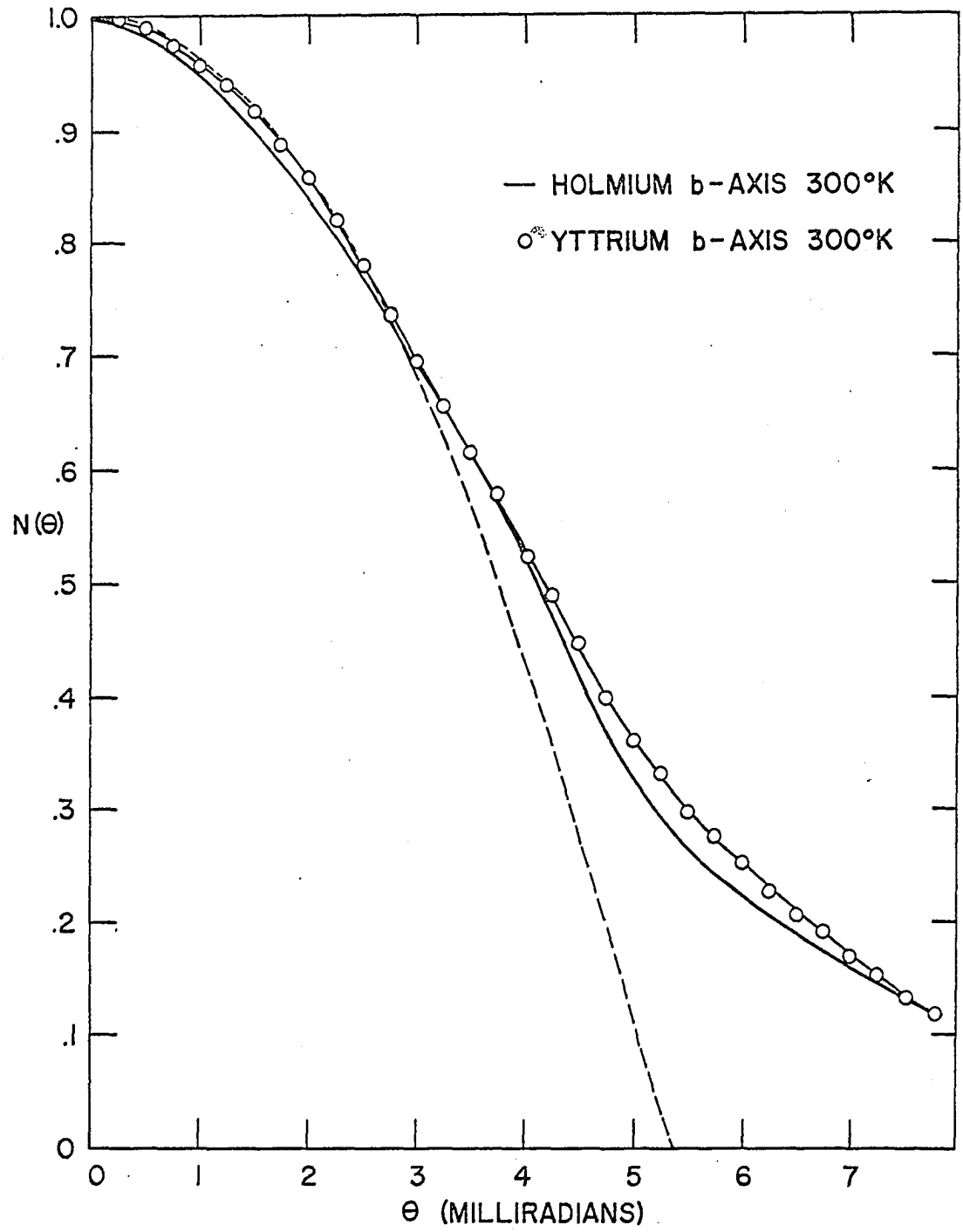


Figure 21. The experimental angular correlation curves of a b-axis (10$\bar{1}$0) holmium crystal and a b-axis yttrium crystal

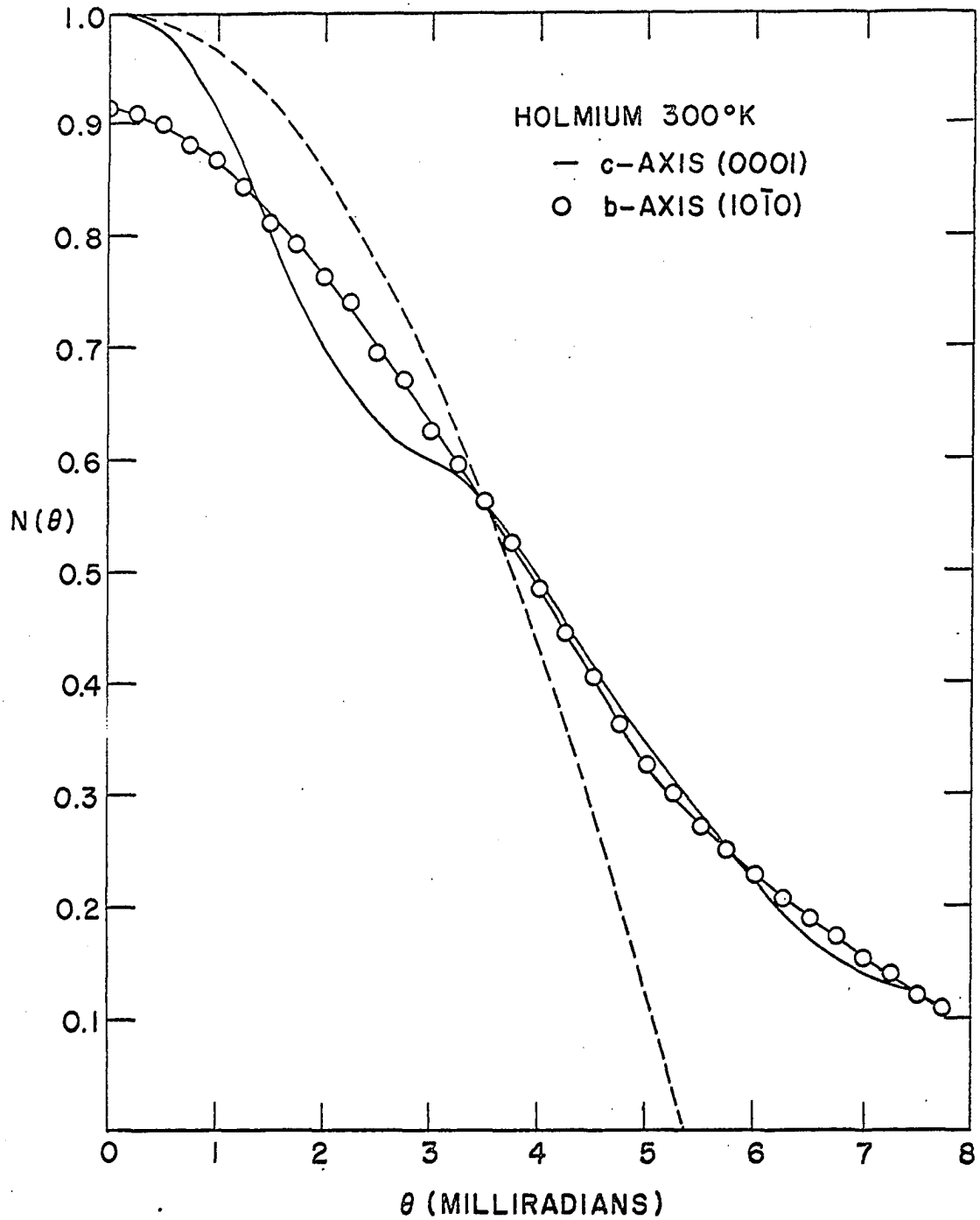


Figure 22. The experimental angular correlation curves of a b-axis (10$\bar{1}$0) and a c-axis (0001) holmium crystal

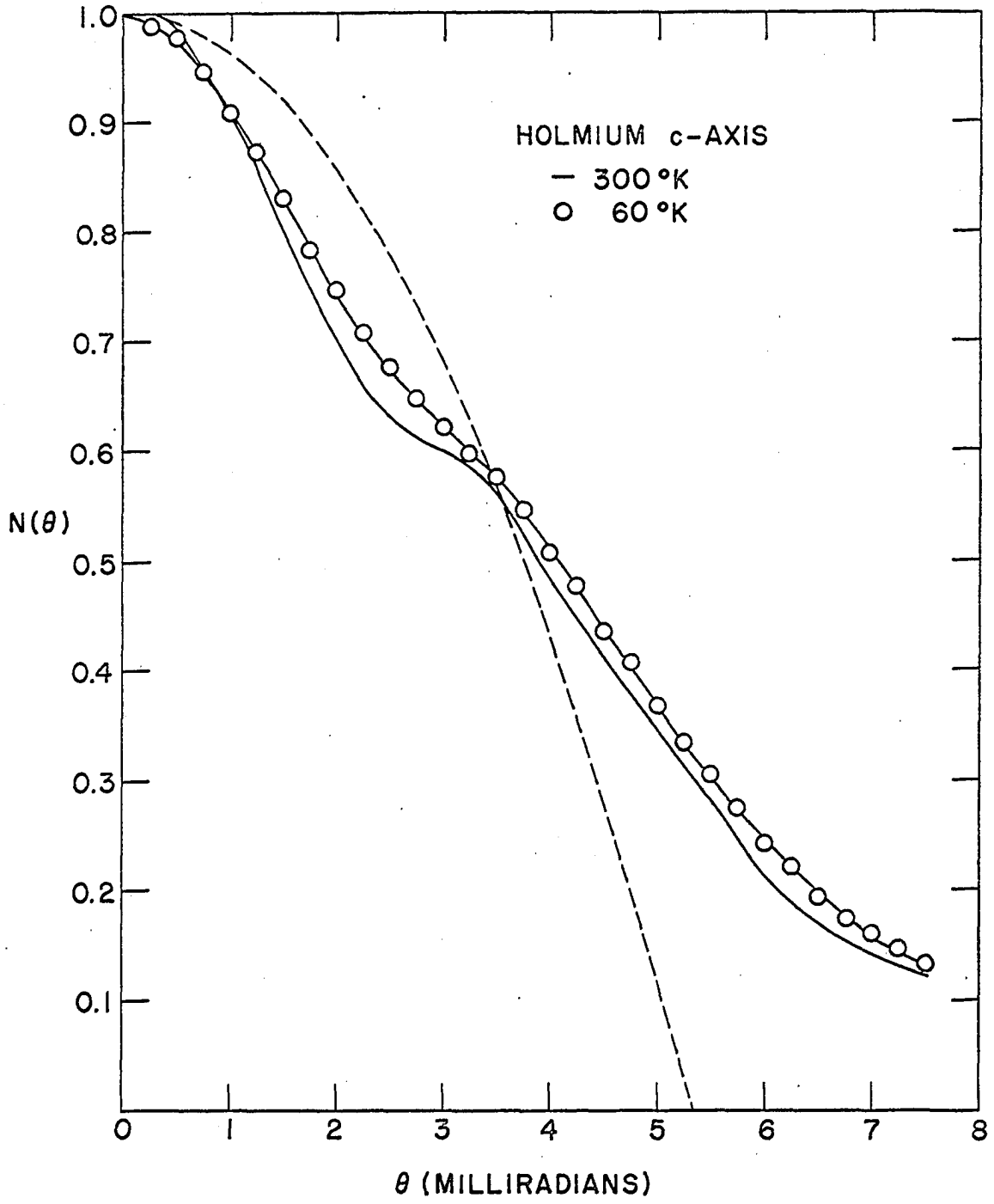


Figure 23. The experimental angular correlation curves of a c-axis (0001) holmium crystal at 300°K and 60°K

ordering has introduced a magnetic super-lattice which has destroyed portions of the Fermi surface. In particular, the ordering has apparently destroyed that part of the surface which causes the hump; that is to say, the flat electron and hole portions of the Fermi surface.

The terbium results and the gadolinium results are shown in Figures 24 and 25. The hump is very small in both curves. These same two curves are compared to the 60°K holmium results in Figure 26. The three curves are almost identical and indicate that those flat portions of the Fermi surface, which are destroyed in holmium when it is magnetically ordered, are not so pronounced in terbium and gadolinium. Since gadolinium does not order antiferromagnetically and terbium does so only over a small temperature range, this indicates clearly that there is a correlation between the occurrence of flat electron and hole regions of Fermi surfaces normal to the c-axis in the metal, and its ability to form a periodic magnetic structure. The gadolinium, terbium, and erbium Fermi surfaces are probably quite similar to the holmium Fermi surface except for modification of the flat portions. There is apparently a tendency for this region to become flatter, and hence increases the tendency towards antiferromagnetic ordering, as one moves across the periodic table from gadolinium to holmium. Indeed, the theoretical band calculations of Loucks and Keeton on dysprosium and holmium (45,46) indicate that these regions do

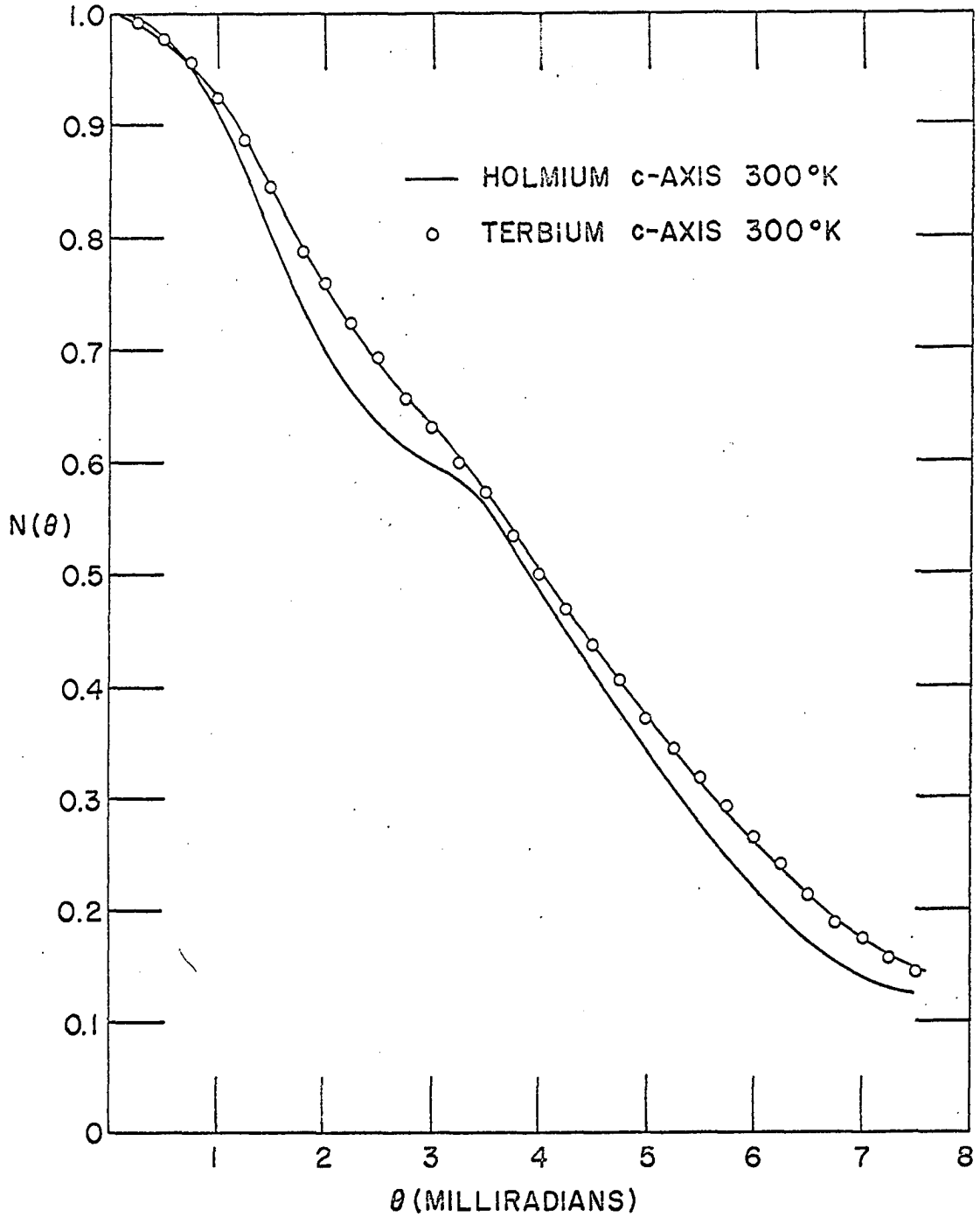


Figure 24. The experimental angular correlation curves of a c-axis (0001) terbium crystal and a c-axis holmium crystal

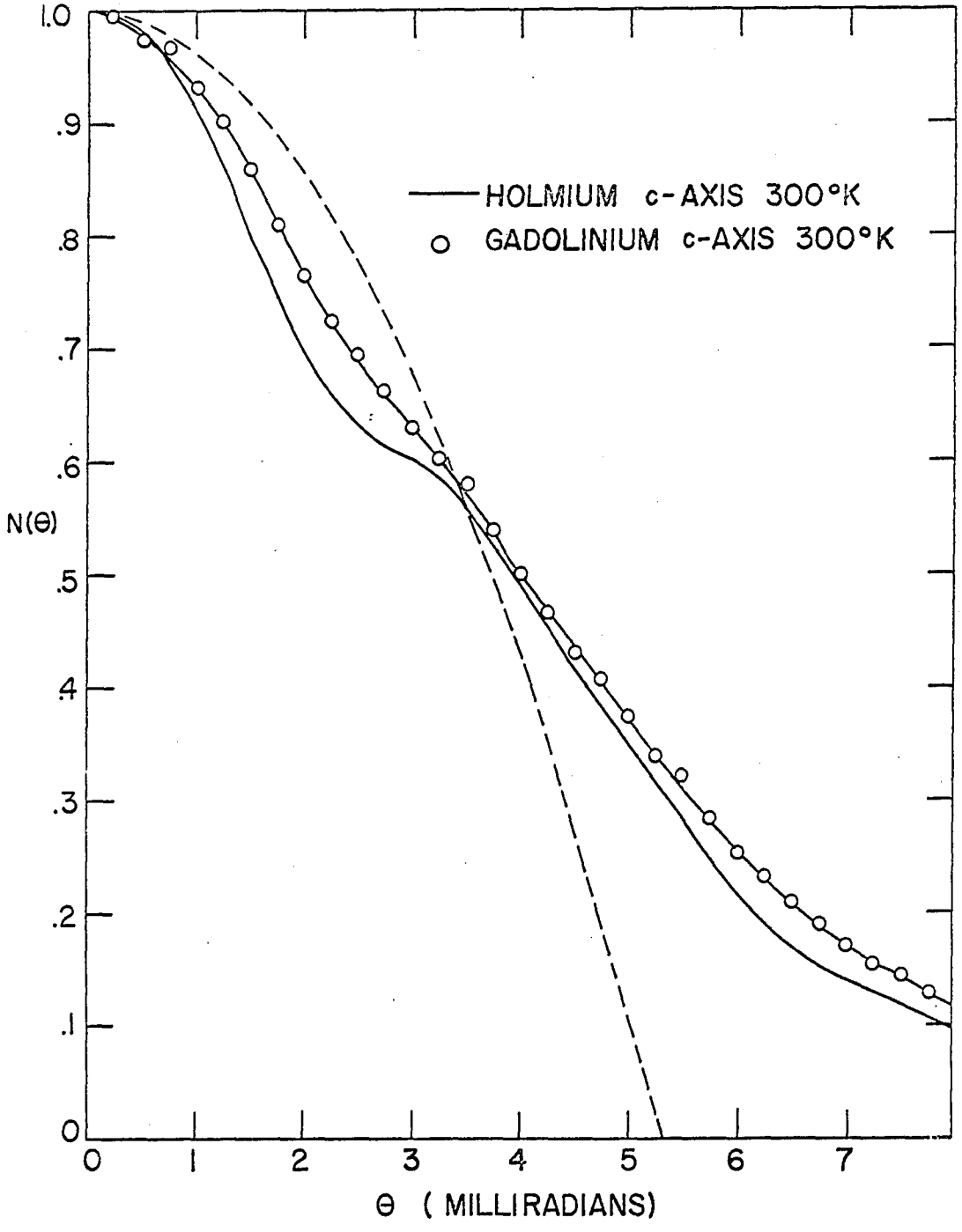


Figure 25. The experimental angular correlation curves of a c-axis (0001) gadolinium crystal and a c-axis holmium crystal

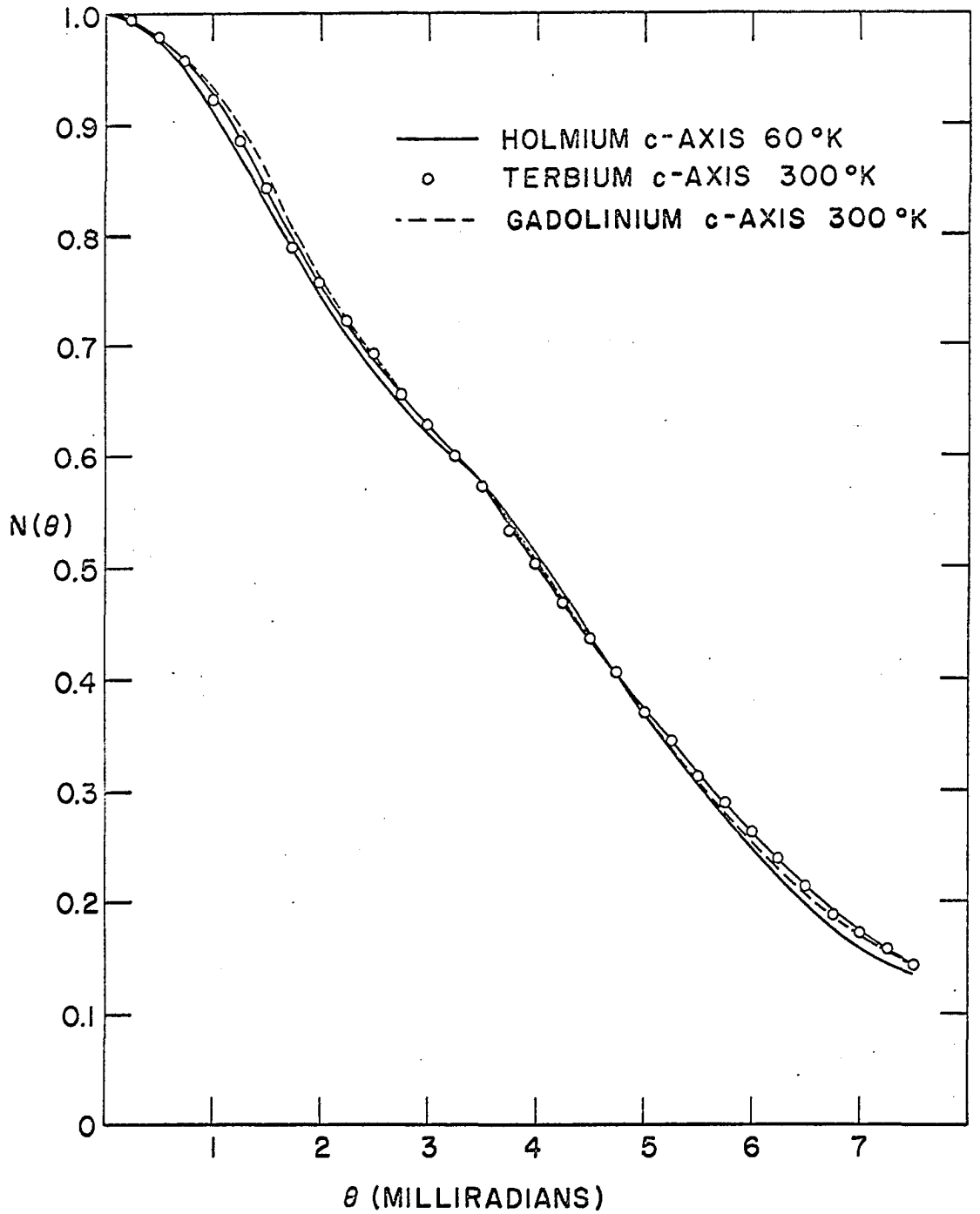


Figure 26. The experimental angular correlation curves of a c-axis (0001) terbium crystal, a c-axis gadolinium crystal and a 60°K c-axis holmium crystal

have a tendency to become flatter. Various experiments also show that gadolinium has no antiferromagnetic structure, that terbium is antiferromagnetic only over a small temperature region, and that the region of antiferromagnetism increases as one continues across the periodic table to dysprosium and holmium (43,47,48). Since erbium and dysprosium also have large regions of antiferromagnetism, comparable to that of holmium, and indicative of large flat regions of their Fermi surface, one might expect a hump in the angular correlation curves. In fact, the erbium and dysprosium curves, shown in Figures 27 and 28 respectively, are almost identical to the holmium curve, as expected.

## The Alloy

An interesting experiment on binary alloys has been carried out by Thoburn et al. (49). These authors have shown that gadolinium-yttrium alloys exhibit antiferromagnetic ordering for alloys having more than 40% yttrium concentration. This observation lends support both to the notion of a Fermi surface in concentrated alloys and to the above arguments on the relation of the flat regions of the Fermi surface to a preferred $\underline{Q}$ vector. Gadolinium has neither antiferromagnetic ordering or flat portions of the Fermi surface, but it does have the prerequisite 4f electrons needed for antiferromagnetic behavior. Conversely, the yttrium does have the flat portions of the Fermi surface, but has no 4f electrons.

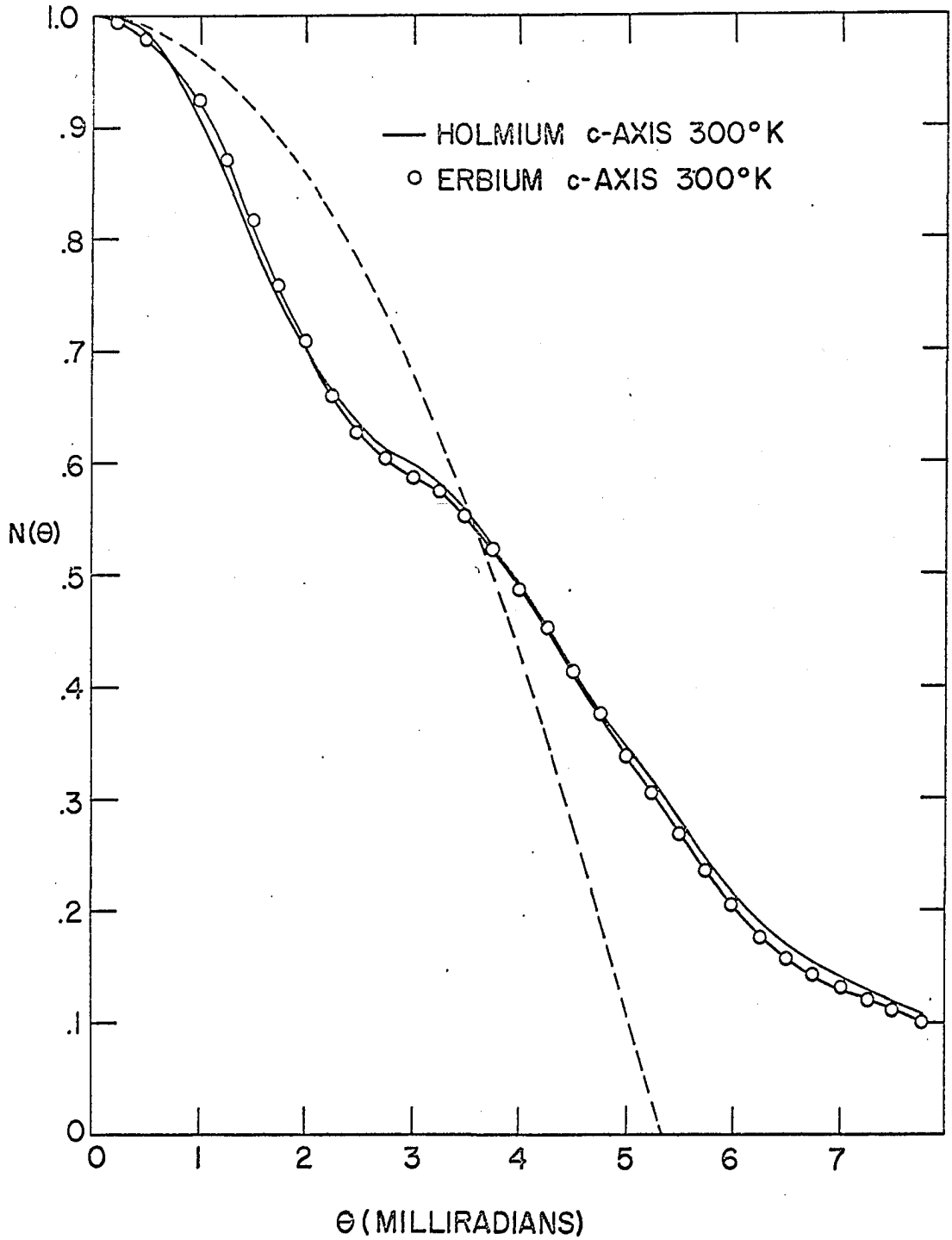


Figure 27. The experimental angular correlation curves of a c-axis (0001) erbium crystal and a c-axis holmium crystal

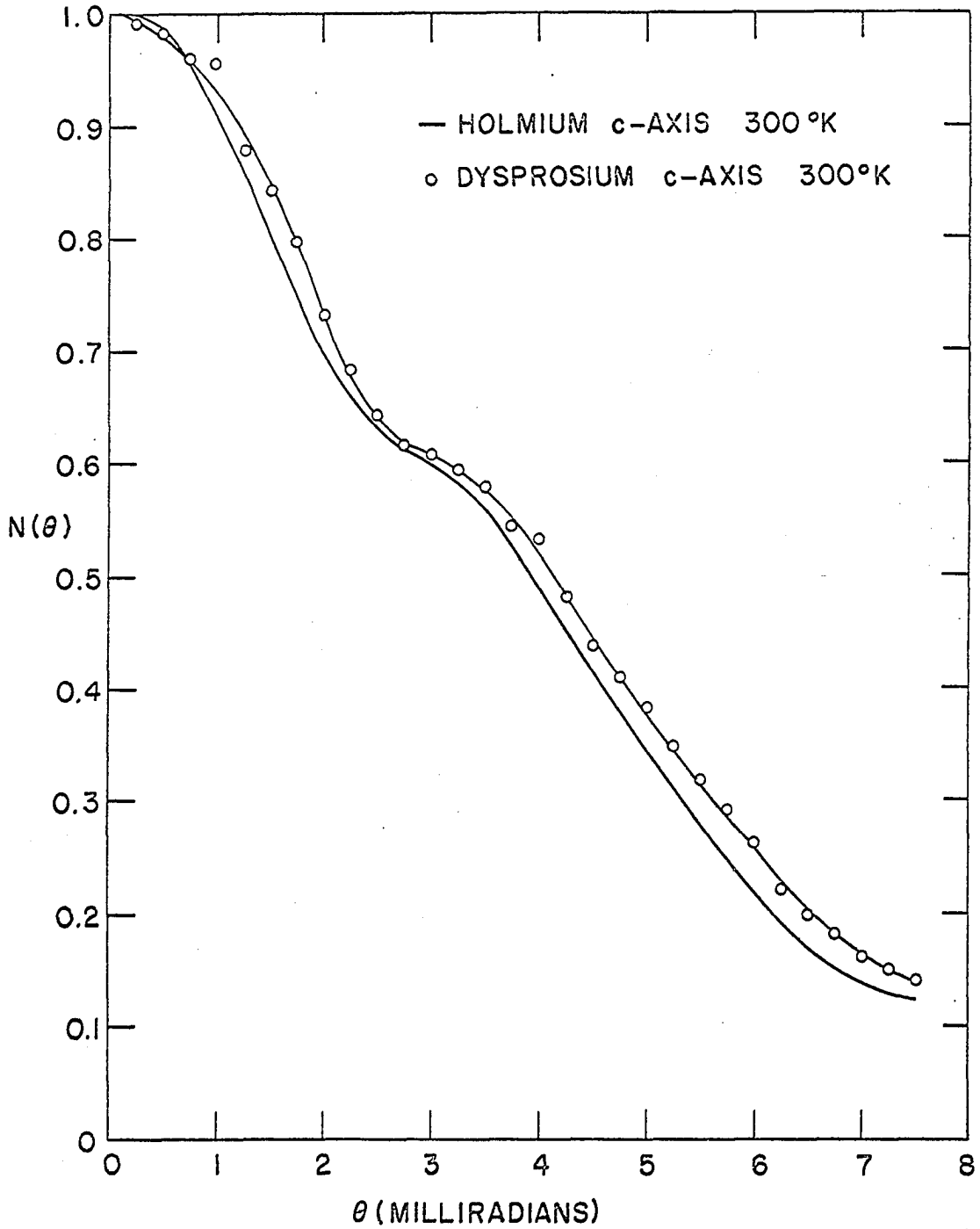


Figure 28. The experimental angular correlation curves of a c-axis (0001) dysprosium crystal and a c-axis holmium crystal

However, since an alloy of the two of these metals exhibits antiferromagnetic ordering, it indicates that the alloy might have a Fermi surface with large, approximately flat hole and electron regions running parallel to one another normal to the c-axis.

What is of equal interest is that it takes only a 31% concentration of scandium, whose conduction electron configuration is similar to the electronic configuration of yttrium and gadolinium, as compared to a 40% concentration of yttrium in gadolinium to cause the resulting alloy to form a spiral structure (50). This seems to indicate that scandium, like yttrium, also might have flat regions of Fermi surface. This in turn suggests that, perhaps, the angular correlation curve for c-axis scandium crystals should have a hump similar to that occurring in yttrium. If it is possible to grow c-axis oriented single crystals of scandium-gadolinium and yttrium-gadolinium alloys then these crystals should show a development of a hump in their angular correlation curves with increasing scandium or yttrium concentrations. Unfortunately, the band structure calculations for scandium, which are needed to check this hypothesis, are at present unavailable.

From experimental results, like those of Nigh et al. (50) and Thoburn et al. (49), it seems reasonable to think of a Fermi surface for concentrated rare earth alloys having similar electronic configuration. With this assumption in mind,

an angular correlation curve for a holmium-50%-erbium c-axis single crystal was experimentally obtained and the results are shown in Figure 29. This figure compares the holmium-50%-erbium results with the holmium c-axis results and shows that the two curves are almost identical. Since erbium differs from holmium only by one additional 4f electron, which is extremely localized at a lattice site and does not overlap on neighboring lattice sites, and since both metals have the same number of electrons and comparable lattice parameters, it seems reasonable to assume that their binary alloy would obey the rigid band model. The experimental results of Figure 29 confirms this expectation. The good correspondence between the alloy's correlation curve and the correlation curves of either of the constituent metals indicates that the Fermi surfaces of all three are quite similar and, consequently, the density of states must also be similar. In particular, the alloy has flat portions of Fermi surface and should exhibit antiferromagnetic ordering. This ordering is experimentally verified by neutron diffraction experiments (51).

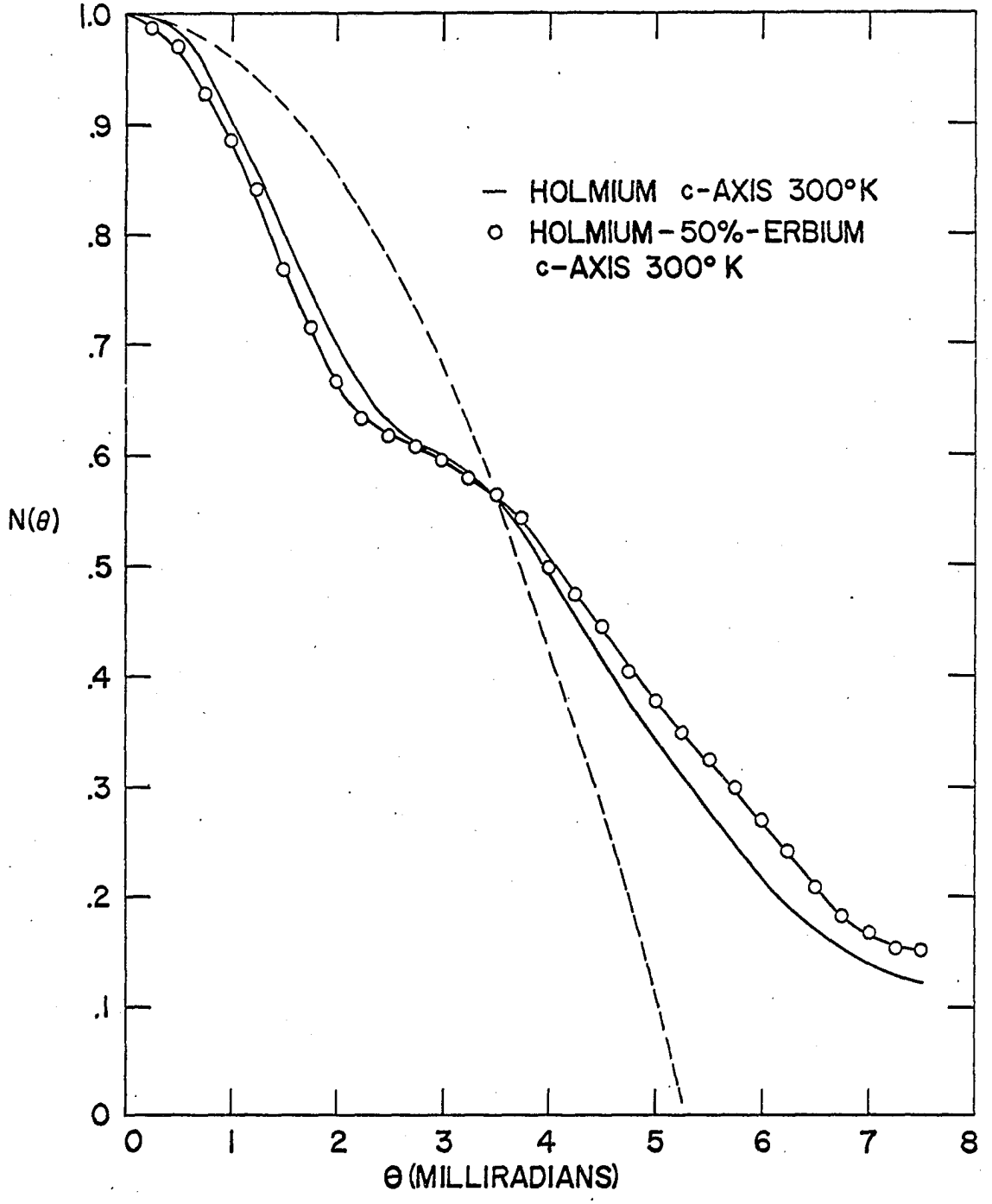


Figure 29. The experimental angular correlation curves of a c-axis (0001) holmium-50%-erbium crystal and a c-axis holmium crystal

# CONCLUSION

In conclusion it has been experimentally demonstrated that the rare earth metals yttrium, gadolinium, terbium, dysprosium, holmium and erbium have highly anisotropic Fermi surfaces.

The experimental angular correlation curve of yttrium has been found to be in qualitative agreement with the theoretical calculations and this supports both the validity of the calculated band structure for yttrium and, as a good first order approximation, the independent particle theory of positron annihilation.

It has been suggested that the hump, which appears in the angular correlation curves of c-axis oriented single crystals of holmium, dysprosium, yttrium and erbium, is due to flat electron and hole regions of the Fermi surface, which run normal to the c-axis and that the comparative lack of such a hump, as in the angular correlation curves of terbium and gadolinium, suggests a modification of this particular feature. The disappearance of this hump in the holmium curve, when the holmium is antiferromagnetically ordered, indicates that the flat portions of the Fermi surface are destroyed on magnetic ordering.

We have observed that several metals which do have flat portions of Fermi surface and, in addition, 4f electrons, exhibit antiferromagnetic ordering and this suggests that such flat regions may be a rather general requirement for the

occurrence of incommensurable, antiferromagnetic structures in metals.

Because of the observed agreement between the yttrium results and the results of the heavy rare earth metals, it is believed that the 4f electrons contribute little to the annihilation process.

Finally, the close similarity between the experimental curves for a holmium-50%-erbium and the experimental curve of holmium and erbium indicates that the Fermi surface is a valid concept for concentrated, binary rare earth alloys and that the rigid band model may apply as a first approximation to holmium-erbium alloys.

Further experimental work could be directed towards determining the angular correlation curves of single crystals of scandium, and, if it is possible to grow such crystals, single crystals of scandium-gadolinium, lanthanum-gadolinium, and yttrium-gadolinium alloys. As it has already been suggested, humps should develop in these alloys as the concentration of solute in gadolinium is increased.

Neutron diffraction and magnetoresistance experiments should be carried out on these same alloys and, in addition, on the binary alloys of the rare earth metals, gadolinium, holmium, erbium, terbium, dysprosium, and lutetium in order to determine their magnetic structures. The rare earth alloy

of lutetium-gadolinium should be of particular interest. Neither gadolinium nor lutetium, having a half filled 4f shell and a filled 4f shell respectively, exhibit antiferromagnetism, but their alloy does (52).

Since gadolinium has no antiferromagnetic structure, it would be interesting to see whether the c-axis gadolinium curve at low temperature is substantially different from that at room temperature. The lack of any large changes would furnish additional proof that it is antiferromagnetic ordering that causes the change in the holmium c-axis curves.

There is a clear need for more band structure calculations on the heavy rare earth metals before the influence of the Fermi surface on antiferromagnetism can be understood in detail.

At the present only one theoretical calculation of the angular correlation curve of a rare earth metal is available. More calculations should be made to further verify that the independent particle model is applicable.

Another series of interesting experiments might be to see what effect changing the s and d electronic structure of hexagonal close packed metals will have on the angular correlation curves. It would be of interest to study, for instance, ruthenium, hafnium and rhenium, which can be obtained in the form of single crystals.

If the formidable mathematical difficulties of the many-

body problem could be overcome, then the effects of electron-positron correlation could be included in the theoretical angular correlation curves. On the experimental side, higher resolution and higher counting rates are necessary before the full potentialities of positron annihilation as a technique for studying the electronic structure of metal can be fully realized.

# BIBLIOGRAPHY


1. Anderson, C. D. The apparent existence of easily deflectable positives. Science, 76, 238 (1932).

2. Sodickson, L., Bowman, W., Stephenson, J, and Weinstein, R. Single-quantum annihilation of positrons. Phys. Rev. 124, 1851 (1961).

3. Glaubman, M., Oberholtzer, J. D., Sheinblatt, M., and Weinstein, R. Single quantum annihilation of positrons. Bull. Am. Phys. Soc. 9, 395 (1964).

4. Rich, J. A. Experimental evidence for the three-photon annihilation of an electron-positron pair. Phys. Rev. 81, 140 (1951).

5. DeBenedetti, S. and Siegel, R. Three-quantum annihilation and positronium. Phys. Rev. 85, 371 (1952).

6. Celitans, G. J. and Green, J. H. Formation and quenching of positronium in gases. I. Results obtained with the three-photon coincidence method. Proc. Phys. Soc. (London) 83, 823 (1964).

7. Beringer, R. and Montgomery, C. G. The angular distribution of positron annihilation radiation. Phys. Rev. 61, 222 (1942).

8. DeBenedetti, S., Cowan, C. E., Konneker, W. R., and Primakoff, H. On the angular distribution of two-photon annihilation radiation. Phys. Rev. 77, 205 (1950).

9. Garwin, R. L. Thermalization of positrons in metals. Phys. Rev. 91, 1571 (1953).

10. Lee-Whiting. Thermalization of positrons in metals. Phys. Rev. 97, 1557 (1955).

11. Bell, R. E. and Graham, R. L. Time distribution of positron annihilation in liquids and solids. Phys. Rev. 90, 644 (1953).

12. Rodda, John Landon, II. Positron mean lives in metals. Unpublished Ph.D. thesis. Ames, Iowa, Library, Iowa State University of Science and Technology (1963).

13. Ferrell, R. A. Theory of positron annihilation in solids. Rev. of Mod. Phys. 28, 308 (1956).

14. Green, R. E. and Stewart, A. T. Angular correlation of photons from positron annihilation in light metals. Phys. Rev. 98, 486 (1955).

15. Stewart, A. T. Angular correlation of photons from positron annihilation in solids. Phys. Rev. 99, 594 (1955).

16. Stewart, A. T. Momentum distribution of metallic electrons by positron annihilation. Can. J. Phys. 35, 168 (1957).

17. Lang, G., DeBenedetti, S., and Smoluchowski, R. Measurement of electron momentum by positron annihilation. Phys. Rev. 99, 596 (1955).

18. Lang, G. and DeBenedetti, S. Angular correlation of annihilation radiation in various substances. Phys. Rev. 108, 914 (1957).

19. Berko, S., Kelley, R. E., Plaskett, J. S. Angular correlation of annihilation radiation from oriented graphite. Phys. Rev. 106, 824 (1957).

20. Berko, S. and Plaskett, J. S. Correlation of Annihilation radiation in oriented single metal crystals. Phys. Rev. 112, 1877 (1958).

21. Stewart, A. T., Shand, J. B., Donaghy, J. J., and Kusmiss, J. H. Fermi surface of beryllium by positron annihilation. Phys. Rev. 128, 118 (1962).

22. Jew, T. T. Magnetic anisotropy in dysprosium single crystals. Unpublished M.S. thesis. Ames, Iowa, Library, Iowa State University of Science and Technology (1963).

23. Strandburg, D. L., Legvold, S., and Spedding, F. H. Electrical and magnetic properties of holmium single crystals. Phys. Rev. 127, 2046 (1962).

24. Mackintosh, A. R. Energy gaps in spin-wave spectra. Phys. Letters 4, 140 (1963).

25. Spedding, F. H., Legvold, S., Daane, A. H., and Jennings, L. D. Some physical properties of the rare earth metals. In C. J. Gorter, ed. Progress in lot temperature physics. Vol. 2. pp. 368-394. Amsterdam, the Netherlands, North-Holland Publishing Company (1957).

26. Behrendt, D. R., Legvold, S., and Spedding, F. H. Magnetic properties of dysprosium single crystals. Phys. Rev. 109, 1544 (1958).

27. Griffel, M., Skochdopole, R. E., and Spedding, F. H. Heat capacity of dysprosium from 15 to 300°K. J. Chem. Phys. 25, 75 (1956).

28. Wilkinson, M. K., Loehler, W. D., Wollan, E. O., and Cable, J. W. Spin configurations. J. Appl. Phys. 32, 48s (1961).

29. Volkenshtein, N. V. and Fedorov, G. V. Temperature dependence of the electrical conductivity and hall effect of dysprosium and erbium. Zh. Eksperim. i Teor. Fiz. 44, 825 (1963). English transl.: Soviet Phys. JETP 17, 560 (1963).

30. Gerstein, B. D., Griffel, M., Jennings, L. D., Miller, R. E., Skochdopole, R. E., and Spedding, F. H. Heat capacity of holmium from 15 to 300°K. J. Chem. Phys. 27, 394 (1957).

31. Koehler, W. C., Cable, J. W., Wollan, E. O., and Wilkinson, M. K. Magnetic structure properties of metallic holmium. Bull. Am. Phys. Soc. 5, 459 (1960).

32. Belov, K. P. and Nikitin, S. A. Galvanomagnetic properties of terbium, dysprosium, and holmium. Fiz. Metal. Metalloved., 13, 43 (1962). English transl.: Physics of Metals and Metallurgy 13, 39 (1962).

33. Sill, L. R. and Legvold, S. Seebeck effect in heavy rare-earth single crystals. Phys. Rev. 137, A1139 (1965).

34. Legvold, S., Alstad, J., and Rhyne, J. Giant magnetostriction in dysprosium and holmium single crystals. Phys. Rev. Letters 10, 509 (1963).

35. Dimmock, J. O. and Freeman, A. J. Band structure and magnetism of gadolinium metal. Phys. Rev. Letters 13, 750 (1964).

36. Mackintosh, A. R. Magnetic ordering and the electronic structure of rare-earth metals. Phys. Rev. Letters 9, 90 (1962).

37. Gustafson, D. R. Positron annihilation in sodium tungsten bronze. Unpublished Ph.D. thesis. Ames, Iowa, Library, Iowa State University of Science and Technology (1964).

38. Nigh, H. E. Magnetization and electrical resistivity of gadolinium single crystals. Unpublished Ph.D. thesis. Ames, Iowa, Library, Iowa State University of Science and Technology (1963).

39. Loucks, T. L. Fermi surface and positron annihilation in yttrium. Phys. Rev. 144, 504 (1966).

40. Slater, J. C. Wave functions in a periodic potential. Phys. Rev. 51, 846 (1937).

41. Ziman, J. M. Principles of the theory of solids. Cambridge University Press, New York, N.Y. (1964).

42. Elliott, R. J. and Wedgwood, F. A. Theory of the resistance of the rare-earth metals. Proc. Phys. Soc. (London) 81, 846 (1963).

43. Elliott, R. J. Phenomenological discussion of magnetic ordering in the heavy rare-earth metals. Phys. Rev. 124, 346 (1961).

44. Liu, S. H. Exchange interaction between conduction electrons and magnetic shell electrons in rare-earth metals. Phys. Rev. 121, 451 (1961).

45. Williams, R. W., Loucks, T. L., and Mackintosh, A. R. Positron annihilation and the electronic structure of rare-earth metals. Phys. Rev. Letters 16, 168 (1966).

46. Keeton, Stewart Charles. Relativistic energy bands and Fermi surfaces for some heavy elements. Unpublished Ph.D. thesis. Ames, Iowa, Library, Iowa State University of Science and Technology (1966).

47. Koehler, W. C. Magnetic properties of rare-earth metals and alloys. J. Appl. Phys. 36, 1078 (1965).

48. Kaplan, T. A. Some effect of anisotropy on spiral spin-configurations with applications to rare earth metals. Phys. Rev. 124, 329 (1961).

49. Thoburn, W. C., Legvold, S., and Spedding, F. H. Magnetic properties of the Gd-La and Gd-Y alloys. Phys. Rev. 110, 1298 (1958).

50. Nigh, H. E., Legvold, S., Spedding, F. H., and Beaudry, B. J. Magnetic properties of Gd-Sc alloys. J. Chem. Phys. 41, 3799 (1964).

51. Shirane, G. and Pickart, S. J. Neutron-diffraction studies of magnetic structures in Ho-Er alloys. J. Appl. Phys. 37, 1032 (1966).

52. Bozorth, R. M. and Gambino, R. J. Magnetic properties of solid solutions of the heavy rare earths with each other. Phys. Rev. 147, 487 (1966).

ACKNOWLEDGEMENT

I would like to thank Dr. A. R. Mackintosh for his suggestion of this problem and for his close guidance and advice in every phase of my graduate career.

Grateful acknowledgement is given to Dr. F. H. Spedding and Mr. B. J. Beaudry who prepared and furnished the rare earth metals used in this investigation.

It is a pleasure to thank Dr. T. L. Loucks for many stimulating and enlightening discussions on the theory of positron annihilation and band structure calculations.

Appreciation is extended to Dr. Sam Legvold and his group for their assistance in growing the rare earth single crystals.

Thanks are due to each of the following for their help in maintaining the electronics: Dr. R. S. Dingus, Mr. W. A. Rhinehart and Mr. R. C. Prior.

# APPENDIX

Table 1. Procedures for the growth of rare earth single crystals

| Metal | Atmosphere | Sample position | Annealing Temperature (°C) | Annealing Time (hrs) |
|---|---|---|---|---|
| Holmium | Argon | Constant temp. | 1300 | 18 |
| Erbium | Argon | " " | 1400 | 18 |
| Yttrium | Vacuum | " " | 1100 | 8 |
| | | " " | 1150 | 8 |
| | | " " | 1200 | 8 |
| | | " " | 1250 | 8 |
| | | " " | 1300 | 8 |
| | | " " | 1350 | 8 |
| Gadolinium | Vacuum | Gradient | 1050 | 12 |
| | | " | 1100 | 12 |
| | | " | 1150 | 12 |
| | | " | 1200 | 12 |
| | | Constant temp. | 1225 | 12 |
| Terbium | Vacuum | " " | 1250 | 12 |
| Holmium-50%-Erbium | Argon | " " | 1350 | 24 |

Table 2. Experimental data for the angular correlation curves of the holmium c-axis (0001) crystal

| Holmium 300°K | | Holmium 60°K | |
|---|---|---|---|
| θ (mrad) | Number of coincidences | θ (mrad) | Number of coincidences |
| 0 | 102664 | 0 | 94162 |
| 0.25 | 102377 | 0.25 | 93205 |
| 0.50 | 101462 | 0.50 | 92148 |
| 0.75 | 97797 | 0.75 | 89265 |
| 1.00 | 93635 | 1.00 | 85540 |
| 1.25 | 88197 | 1.25 | 82212 |
| 1.50 | 82375 | 1.50 | 78219 |
| 1.75 | 77157 | 1.75 | 73770 |
| 2.00 | 72064 | 2.00 | 70248 |
| 2.25 | 67696 | 2.25 | 66535 |
| 2.50 | 64735 | 2.50 | 63670 |
| 2.75 | 62940 | 2.75 | 61151 |
| 3.00 | 61546 | 3.00 | 58500 |
| 3.25 | 60111 | 3.25 | 56439 |
| 3.50 | 57469 | 3.50 | 54267 |
| 3.75 | 53940 | 3.75 | 51501 |
| 4.00 | 50860 | 4.00 | 47910 |
| 4.25 | 46428 | 4.25 | 45030 |
| 4.50 | 42198 | 4.50 | 41097 |
| 4.75 | 38991 | 4.75 | 38290 |
| 5.00 | 35618 | 5.00 | 34604 |
| 5.25 | 32554 | 5.25 | 31584 |
| 5.50 | 28873 | 5.50 | 28756 |
| 5.75 | 25694 | 5.75 | 25938 |
| 6.00 | 22353 | 6.00 | 22963 |
| 6.25 | 19279 | 6.25 | 20895 |
| 6.50 | 17343 | 6.50 | 18445 |
| 6.75 | 15770 | 6.75 | 16568 |
| 7.00 | 14623 | 7.00 | 15291 |
| 7.25 | 13322 | 7.25 | 13774 |
| 7.50 | 12346 | 7.50 | 12601 |
| 7.75 | 11080 | 7.75 | 11398 |
| 8.00 | 10065 | 8.00 | 10029 |

Table 3. Experimental data for the angular correlation curves of the holmium b-axis (10$\bar{1}$0) and the yttrium b-axis crystals

| Holmium 300°K | | Yttrium 300°K | |
|---|---|---|---|
| θ (mrad) | Number of coincidences | θ (mrad) | Number of coincidences |
| 0 | 61199 | 0 | 63655 |
| 0.25 | 61046 | 0.25 | 63121 |
| 0.50 | 60330 | 0.50 | 62590 |
| 0.75 | 59102 | 0.75 | 62069 |
| 1.00 | 58138 | 1.00 | 60899 |
| 1.25 | 56451 | 1.25 | 59953 |
| 1.50 | 54365 | 1.50 | 58307 |
| 1.75 | 53141 | 1.75 | 56459 |
| 2.00 | 51263 | 2.00 | 54468 |
| 2.25 | 49675 | 2.25 | 52319 |
| 2.50 | 46660 | 2.50 | 49644 |
| 2.75 | 45006 | 2.75 | 46696 |
| 3.00 | 41992 | 3.00 | 44197 |
| 3.25 | 40025 | 3.25 | 41810 |
| 3.50 | 37768 | 3.50 | 38890 |
| 3.75 | 35359 | 3.75 | 36216 |
| 4.00 | 32499 | 4.00 | 33239 |
| 4.25 | 29867 | 4.25 | 30065 |
| 4.50 | 27305 | 4.50 | 26813 |
| 4.75 | 24372 | 4.75 | 23459 |
| 5.00 | 22044 | 5.00 | 20873 |
| 5.25 | 20325 | 5.25 | 18572 |
| 5.50 | 18206 | 5.50 | 16964 |
| 5.75 | 16968 | 5.75 | 15494 |
| 6.00 | 15398 | 6.00 | 14338 |
| 6.25 | 13935 | 6.25 | 13249 |
| 6.50 | 12644 | 6.50 | 12276 |
| 6.75 | 11693 | 6.75 | 11139 |
| 7.00 | 10383 | 7.00 | 10529 |
| 7.25 | 9371 | 7.25 | 9314 |
| 7.50 | 8175 | 7.50 | 8400 |
| 7.75 | 7523 | 7.75 | 7748 |
| 8.00 | 6635 | 8.00 | 7038 |

Table 4. Experimental data for the angular correlation curves of the terbium c-axis (0001) and the gadolinium c-axis crystals

| Terbium | | Gadolinium | |
|---|---|---|---|
| θ (mrad) | Number of coincidences | θ (mrad) | Number of coincidences |
| 0 | 50,824 | 0 | 26,777 |
| 0.25 | 50,490 | 0.25 | 26,727 |
| 0.50 | 49,752 | 0.50 | 26,075 |
| 0.75 | 48,676 | 0.75 | 25,950 |
| 1.00 | 46,927 | 1.00 | 24,938 |
| 1.25 | 45,056 | 1.25 | 24,112 |
| 1.50 | 42,919 | 1.50 | 22,978 |
| 1.75 | 40,032 | 1.75 | 21,693 |
| 2.00 | 38,539 | 2.00 | 20,487 |
| 2.25 | 36,743 | 2.25 | 19,341 |
| 2.50 | 35,206 | 2.50 | 18,581 |
| 2.75 | 33,265 | 2.75 | 17,760 |
| 3.00 | 31,989 | 3.00 | 16,953 |
| 3.25 | 30,488 | 3.25 | 16,124 |
| 3.50 | 24,036 | 3.50 | 15,550 |
| 3.75 | 27,127 | 3.75 | 14,437 |
| 4.00 | 25,433 | 4.00 | 13,358 |
| 4.25 | 23,762 | 4.25 | 12,455 |
| 4.50 | 22,144 | 4.50 | 11,581 |
| 4.75 | 20,573 | 4.75 | 10,899 |
| 5.00 | 18,819 | 5.00 | 10,012 |
| 5.25 | 17,500 | 5.25 | 9,055 |
| 5.50 | 16,094 | 5.50 | 8,619 |
| 5.75 | 14,846 | 5.75 | 7,600 |
| 6.00 | 13,370 | 6.00 | 6,811 |
| 6.25 | 12,198 | 6.75 | 6,237 |
| 6.50 | 10,840 | 7.00 | 5,639 |
| 6.75 | 9,563 | 7.25 | 5,087 |
| 7.00 | 8,851 | 7.50 | 4,616 |
| 7.25 | 7,950 | 7.75 | 4,154 |
| 7.50 | 7,221 | 8.00 | 3,881 |
| 7.75 | 6,651 | | |
| 8.00 | 6,056 | | |

Table 5. Experimental data for the angular correlation curves of the erbium c-axis (0001) and the yttrium c-axis crystals

| Erbium 300°K | | Yttrium 300°K | |
|---|---|---|---|
| θ (mrad) | Number of coincidences | θ (mrad) | Number of coincidences |
| 0 | 127,759 | 0 | 83,093 |
| 0.25 | 126,860 | 0.25 | 82,838 |
| 0.50 | 124,629 | 0.50 | 81,403 |
| 0.75 | 119,888 | 0.75 | 78,674 |
| 1.00 | 114,527 | 1.00 | 76,833 |
| 1.25 | 106,934 | 1.25 | 72,404 |
| 1.50 | 98,266 | 1.50 | 67,999 |
| 1.75 | 89,386 | 1.75 | 63,010 |
| 2.00 | 82,767 | 2.00 | 58,677 |
| 2.25 | 78,415 | 2.25 | 54,729 |
| 2.50 | 76,966 | 2.50 | 52,037 |
| 2.75 | 75,908 | 2.75 | 50,283 |
| 3.00 | 74,030 | 3.00 | 48,819 |
| 3.25 | 71,619 | 3.25 | 47,743 |
| 3.50 | 67,875 | 3.50 | 45,903 |
| 3.75 | 63,695 | 3.75 | 43,615 |
| 4.00 | 57,954 | 4.00 | 40,479 |
| 4.25 | 52,734 | 4.25 | 37,524 |
| 4.50 | 47,184 | 4.50 | 34,031 |
| 4.75 | 42,961 | 4.75 | 31,206 |
| 5.00 | 37,830 | 5.00 | 28,078 |
| 5.25 | 32,501 | 5.25 | 25,464 |
| 5.50 | 27,868 | 5.50 | 22,443 |
| 5.75 | 23,349 | 5.75 | 19,796 |
| 6.00 | 19,632 | 6.00 | 17,084 |
| 6.25 | 17,574 | 6.25 | 14,691 |
| 6.50 | 15,768 | 6.50 | 13,112 |
| 6.75 | 14,595 | 6.75 | 12,049 |
| 7.00 | 13,639 | 7.00 | 10,884 |
| 7.25 | 12,659 | 7.25 | 9,995 |
| 7.50 | 11,659 | 7.50 | 9,206 |
| 7.75 | 10,500 | 7.75 | 8,350 |
| 8.00 | 9,596 | 8.00 | 7,407 |

Table 6. Experimental data for the angular correlation curve of the erbium-50%-holmium c-axis (0001) crystal

| θ (mrad) | Number of coincidences |
|---|---|
| 0 | 48458 |
| 0.25 | 47870 |
| 0.50 | 47037 |
| 0.75 | 44955 |
| 1.00 | 42917 |
| 1.25 | 40744 |
| 1.50 | 37288 |
| 1.75 | 34686 |
| 2.00 | 32373 |
| 2.25 | 30758 |
| 2.50 | 29939 |
| 2.75 | 29448 |
| 3.00 | 28794 |
| 3.25 | 28044 |
| 3.50 | 27267 |
| 3.75 | 26272 |
| 4.00 | 24105 |
| 4.25 | 22925 |
| 4.50 | 21568 |
| 4.75 | 19500 |
| 5.00 | 18280 |
| 5.25 | 16869 |
| 5.50 | 15698 |
| 5.75 | 14459 |
| 6.00 | 12996 |
| 6.25 | 11633 |
| 6.50 | 9993 |
| 6.75 | 8791 |
| 7.00 | 8138 |
| 7.25 | 7478 |
| 7.50 | 7490 |

Table 7. Theoretical data for the angular correlation curve of the yttrium c-axis (0001)

| θ (mrad) | Number of coincidences |
|---|---|
| 0.108 | 1.000 |
| 0.324 | 0.993 |
| 0.540 | 0.988 |
| 0.756 | 0.960 |
| 0.972 | 0.930 |
| 1.188 | 0.900 |
| 1.404 | 0.818 |
| 1.620 | 0.677 |
| 1.836 | 0.638 |
| 2.052 | 0.571 |
| 2.269 | 0.562 |
| 2.485 | 0.609 |
| 2.701 | 0.597 |
| 2.917 | 0.550 |
| 3.133 | 0.532 |
| 3.349 | 0.481 |
| 3.565 | 0.460 |
| 3.782 | 0.440 |

Table 8. Experimental data for the angular correlation curve of the dysprosium c-axis (0001) crystal

| θ (mrad) | Number of coincidences |
|---|---|
| 0 | 17333 |
| 0.25 | 17172 |
| 0.50 | 17020 |
| 0.75 | 16654 |
| 1.00 | 16563 |
| 1.25 | 15236 |
| 1.50 | 14614 |
| 1.75 | 13838 |
| 2.00 | 12669 |
| 2.25 | 11820 |
| 2.50 | 11117 |
| 2.75 | 10670 |
| 3.00 | 10505 |
| 3.25 | 10285 |
| 3.50 | 10005 |
| 3.75 | 9412 |
| 4.00 | 9242 |
| 4.25 | 8325 |
| 4.50 | 7611 |
| 4.75 | 7109 |
| 5.00 | 6629 |
| 5.25 | 6047 |
| 5.50 | 5525 |
| 5.75 | 5057 |
| 6.00 | 4555 |
| 6.25 | 3828 |
| 6.50 | 3448 |
| 6.75 | 3152 |
| 7.00 | 2794 |
| 7.25 | 2595 |
| 7.50 | 2423 |
| 7.75 | 2225 |
| 8.00 | 2008 |